2020

On-Demand Electrically Induced Decomposition of Thin-Film Nitrocellulose Membranes for Wearable or Implantable Biosensor Systems

Benjamin M. Horstmann
Virginia Commonwealth University

On-Demand Electrically Induced Decomposition of Thin-Film Nitrocellulose Membranes for Wearable or Implantable Biosensor Systems

A thesis submitted in partial fulfillment of the requirements for the degree of Master of Science in Electrical Engineering at Virginia Commonwealth University.

by

Benjamin Mark Horstmann

Bachelor of Science in Nuclear Engineering Technology, Excelsior College, 2012

Bachelor of Science in Electrical Engineering, Virginia Commonwealth University, 2017

Director: Vitaliy Avrutin,

Associate Professor, Department of Electrical and Computer Engineering

Virginia Commonwealth University
Richmond, Virginia
May, 2020

Acknowledgments

The author wishes to thank several people.

First and most importantly, I would like to thank my wife, Joanna, and my daughters, Jillian and Brianna, for their love, support and patience.

I would like to thank my thesis advisor Professor Vitaliy Avrutin, to whom I owe a great deal. I have gained a respect for the small details and a better understanding of how to look at a problem from all angles.

I would also like to thank my other advisory committee members, Professor Ümit Özgür and Professor Vamsi Yadavalli. Without their support, patience, and guidance this would not have been possible.

I would like to specifically thank Dr. Kai Ding for any and all guidance and teaching he has provided.

I would also like to thank all the colleagues that helped me throughout this entire process. Specifically, Kosuke Yokoyama for bouncing ideas off of and for help in the clean room. All of my colleagues have kept me sane and always provide interesting conversations.

Lastly, I would like to thank my parents, who have both passed, who were always there for me and pushed me to be a better person.

Table of Contents Page

List of Figures

Page

List of Tables

Abstract

Implantable or subcutaneous biosensors used for continuous health monitoring have a limited functional lifetime requiring frequent replacement and therefore may be highly discomforting to the patient and become costly. One possible solution to this problem is use of biosensor arrays where each individual reserve sensor can be activated on-demand when the previous one becomes inoperative due to biofouling or enzyme degradation. Each reserve biosensor in the array is housed in an individual Polydimethylsiloxane (PDMS) well and is protected from exposure to bodily fluids such as interstitial fluid (ISF) by a thin-film nitrocellulose membrane. Controlled activation is achieved by decomposing over an individual sensor well. Electrically activated thermal decomposition of the nitrocellulose membrane is caused by passing an electric current through an Au/Ti filament placed on top of the membrane. By applying an energy of as low as 7 mJ to the Au/Ti filament with cross-sectional area of 8 x 10^7 cm^2, a current density of $\approx 10^5 - 10^6$ A/cm^2 causes explosive decomposition of thin-film Au/Ti filaments. Having a thermal decomposition temperature of ≈200°C, nitrocellulose is locally heated directly under the Au/Ti filament. This leads to opening of the nitrocellulose membrane within 50 ms allowing for exposure of biosensor to biofluids. 50 ms is sufficiently short to prevent local heating of surrounding tissues and therefore is not a danger to a potential patient.

Vita

Ben Horstmann received his Bachelor of Science degree in Nuclear Engineering Technology from Excelsior College in 2012. He also received his Bachelor of Science degree in Electrical Engineering from Virginia Commonwealth University in 2017.

He entered the Graduate program in the Department of Electrical Engineering at Virginia Commonwealth University in September 2017 and received his Master of Science degree in May 2020. His research interests include microfluidics, solar cell designs and fabrication processes.

Mr. Ben Horstmann may be reached at 4819 Kipper Dr., Moseley, VA 23120. His email is bhorstmann77@gmail.com.

1 INTRODUCTION/MOTIVATION

Long-term continuous health monitoring has become a necessity in the ever-growing healthcare industry [1]. This leads to a shift towards preventative methods versus reactionary methods of old. With this new preventative mindset, biosensors have become instrumental in detection and monitoring of many different health problems [1].

Biosensors used for point-of-care (POC) testing in the healthcare industry have become useful for relatively quick and accurate patient health diagnoses. Some examples of biosensor based POC tests include blood glucose monitors, home pregnancy tests, and illicit drug discovery [1]. Blood glucose monitors are one of the most employed POC tests for long-term patient health monitoring and the other examples, home pregnancy tests and illicit drug discovery, are still widely used but are considered short-term or single-use type of biosensors. A brief introduction of the operation and components utilized in a general biosensor will be discussed in Section 2.1.1 and described in more detail concerning glucose biosensing in Section 2.1.2. There are a multitude of different biosensor and target analytes that could be utilized with glucose sensing as one good option for integration with our solution.

Almost 6% of the approximate 7.5 billion people worldwide suffer from Diabetes Mellitus (commonly known as Diabetes) [2][3]. For Type I diabetics, continuous health monitoring is required to avoid low blood sugar (hypoglycaemia) situations. Therefore, in the early 1960's, Leland and Clark [4] invented Clark-type biosensors giving patients the ability to monitor their glycaemia levels multiple times throughout a day. With each test, the patient would determine how much insulin is required to inject into themselves and thereby control their blood sugar levels.

Through this controlled monitoring, patients are better able to control their diabetic hypoglycaemic (low blood sugar) and hyperglycaemic (high blood sugar) episodes.

Within the last two decades, better control methods have risen in the form of continuous glucose monitoring [5]. However, functional lifetime of each biosensor is relatively short. 3 to 7 days is the typical lifetime and changing the sensor can become very expensive and discomforting for the patient [5]. Recently, commercial CGM devices such as the Freestyle Libre have been reported to last up to 14 days [6]. Additionally, shortages of these sensors have occurred recently in the UK as reported by BBC [7]. There have also been reports of an implantable optical sensor made by Eversense [8] that can extend the functional lifetime to 90 days (US Version). However, the sensitivity of this optical sensor is lacking in the hypoglycaemic range.

A possible solution to this sensor lifetime and shortage problem is to create an array of biosensors that can be activated on-demand when needed. All of the biosensors are protected from premature biofouling by a protective membrane that can be sequentially and rapidly removed to expose and activate a particular biosensor as needed. By using an array of biosensors, the effective lifetime would be increased significantly leading to reduced discomfort to the patient and lower potential cost for the patient. Additionally, shortages could be curtailed as well.

A conceptual design for a small array of biosensors can be seen in Fig. 1.1. Using an array of biosensors requires precise control over each biosensor's activation. Use of energetic polymers to not only protect all biosensors but also allow for a decomposition mechanism to give access of biofluids to each biosensor is the method of choice for this work. The energetic polymer chosen is nitrocellulose (NC) which gives rupturable protective membranes that can be controlled. NC reacts exothermically with heat applied and rapidly decomposes. After decomposition, the membrane which was preventing biofluids such as interstitial fluid (ISF) is now gone and biofluids interact

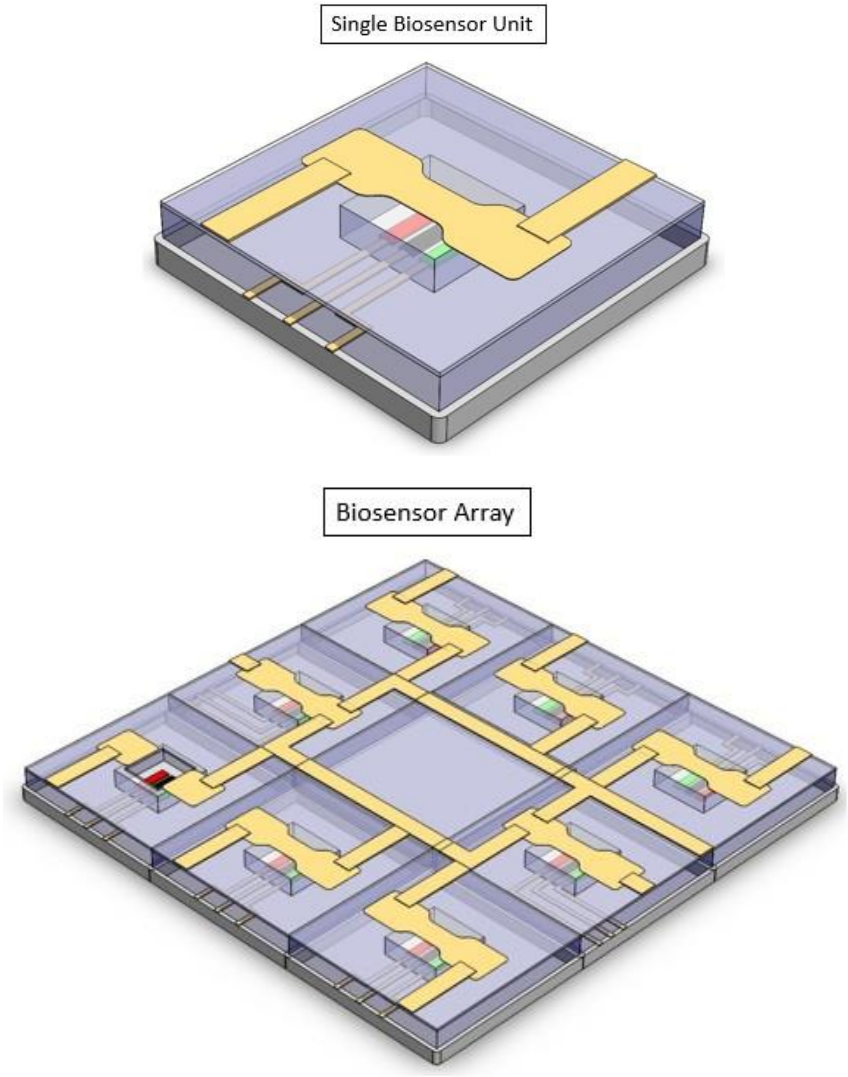

Figure 1.1 *Conceptual designs of the proposed sensor in a single well on top and an array of sensors on bottom with one activated biosensor. 3D view of design viewing down into Polydimethylsiloxane (PDMS) well structures to biosensor. A three-electrode electrochemical sensor is shown as an example with GREEN being the counter electrode,* ***BLACK*** *being the reference electrode, and RED being the working electrode. Bow tie-shaped Au/Ti filaments deposited on nitrocellulose membrane over each well structure to initiate activation. Au/Ti trace lines make connections to ground side of Au/Ti filaments. Alternate side of filaments used to apply current through Au/Ti filament.*

with and activate the biosensor. Variants of this process were originally proposed for drug delivery using alternate protective membranes formed from Au [9] and Pt/Ti/Pt [12].

NC is known to be an explosive and propellant [5]. Fig. 1.2 shows a sample of fibrous NC that resembles a cotton ball but is actually a piece of nitrated cotton giving it explosive properties.

Figure 1.2 *Sample of fibrous NC resembling a cotton ball.*

Deposition of Titanium (Ti) and Gold (Au) via Electron-Beam and Thermal Evaporation on to NC will act as a contact or filament. Ti acts as an adhesion layer and Au acts as the filament or contact. By applying a current flow through this filament, the filament will increase local temperature of NC to its critical decomposition temperature. When NC decomposes over a well structure, biofluids will have access to perform continuous health monitoring via a biosensor housed within the well structure. This can be better visualized in the cross-sectional view shown in Fig. 1.3 and in conceptual designs shown in Fig. 1.4 showing comparison of an active well with a biofluid (ISF) versus an un-fouled inactive well.

This work seeks to determine the appropriate amount of current, power, and energy to decompose NC. Also, understanding of how thickness of NC affects this decomposition is important. To test these NC membranes, a method deriving benefit from applying large current densities to thin-film Au/Ti filaments was exploited.

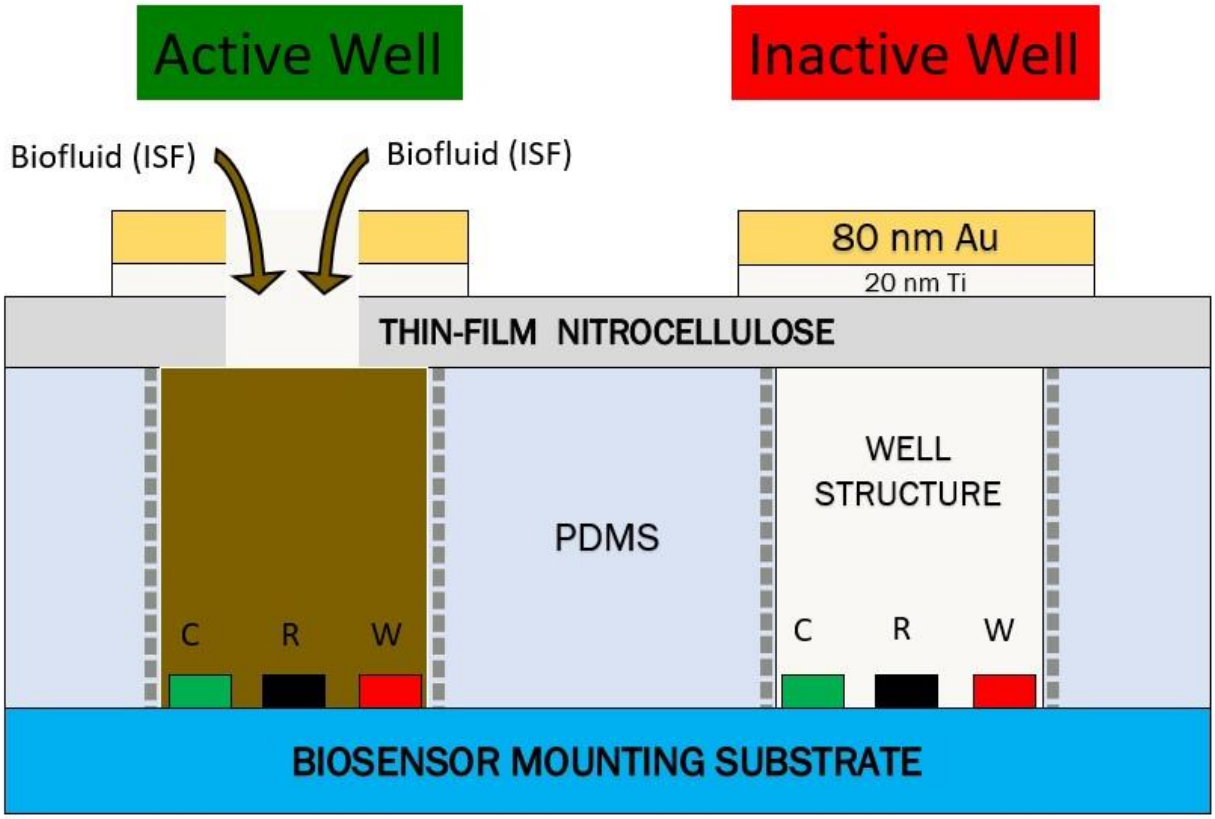

Figure 1.3 *Cross-section schematic of the proposed sensor design. Starting from the bottom, a biosensor is mounted to the bottom of the PDMS well structures. A three-electrode sensor is shown as an example with C being the counter electrode, R being the reference electrode, and W being the working electrode. Next, a thin film of NC is bonded to the top side acting as access control for biofluids. Finally, bow tie-shaped Au/Ti filaments are deposited on the NC membrane over each well structure. 20 nm of Ti film serves as an adhesion layer for the 80 nm Au filament. Additionally, a comparison between an Active well with NC decomposed to an Inactive well is shown. In the Active well, biofluid (ISF) has entered into the well activating the biosensor.*

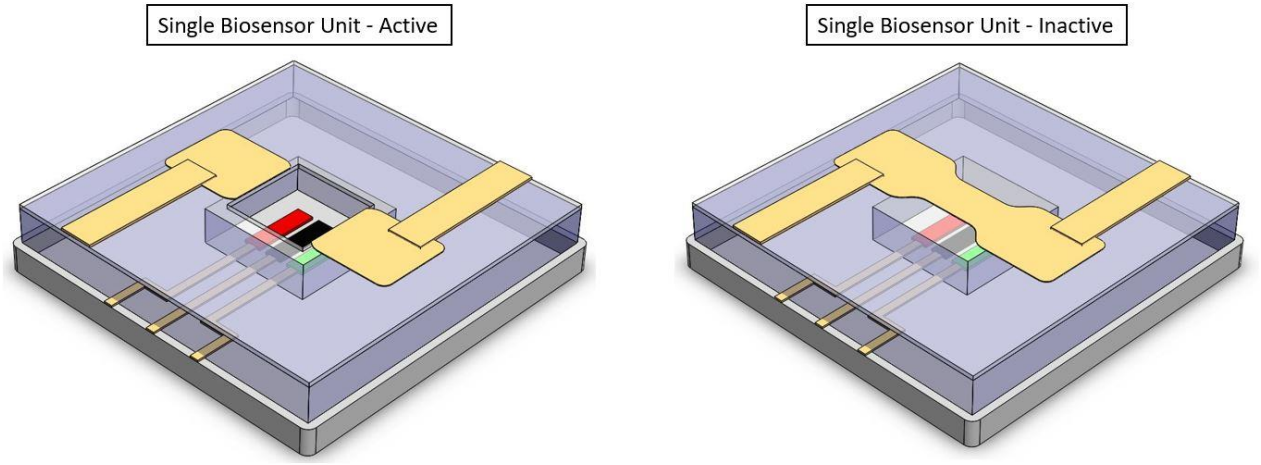

Figure 1.4 *Comparison between an Active well with NC decomposed to an Inactive well with Au/Ti filament and thin film NC membrane intact. NC membrane prevents the biosensor from being biofouled until use of the biosensor is required.*

Normally, low currents are applied to thin-film Au/Ti filaments for many other applications. However, a strong, violent reaction occurs when ample current is applied to thin Au filaments. The Au/Ti filament will undergo an explosive decomposition. This will be described in more detail in section 2.4 with a literature review of explosively decomposing different metal wires and thin-films [9][42][43][44][45][46][47].

Testing of the decomposition of NC is done in two different systematic ways. The first, as presented in Section 4.2, systematically tests the decomposition of NC directly on a Platinum (Pt) covered Sapphire wafer using Au/Ti filaments atop the NC. The second, as presented in Section 4.3, systematically tests the decomposition of NC transferred to polydimethylsiloxane (PDMS) well structures using Au/Ti filaments again. The PDMS well structure fabrication will be described in Section 3.2.

Also, as this has long–term biomedical applications, porosity of NC membranes is to be tested to ensure NC will not leak if implanted into a patient. If a system is developed to deliver drugs to a certain area, a leak from a NC membrane could cause significant health issues for the patient. Therefore, leak testing is performed and results are shown in Section 4.4.

Additionally, as a future work, the long-term biocompatibility of NC must be determined in in vivo conditions. It is known that NC is widely used in western blot testing (nucleic acid and protein detection) due to its capability to strongly adsorb biomolecules through electrostatic, hydrophobic and hydrogen interactions [10]. Li et. al [11] determined that NC acting as a scaffold for cell growth showed a low cytotoxicity and high cytocompatibility. This is promising for our work but long-term biocompatibility testing must still be performed to determine if implantation will be an issue or not.

A review of related chemical and thermal properties of NC will be discussed in Section 2.3 and 2.4. Before discussing results of the systematic testing, design and test requirements must be defined and are described in Section 3.1. Next, in Sections 3.2, 3.3 and 3.4, fabrication of key components is described. Section 3.3 will also establish spin curves for spin-coating NC onto a substrate at a required thickness. More common procedures such as mixing PDMS can be accessed from their respective datasheets and will be briefly described in Appendix B. In Section 3.5, design challenges are briefly discussed to understand the limitations of this configuration. Then, as mentioned previously, systematic testing is described in Sections 4.1, 4.2, 4.3, and 4.4. Section 4.1 will address the experimental test bench setup. Lastly, a brief discussion on the results and the future of our work.

2 BACKGROUND AND THEORY

2.1 BIOSENSOR DESCRIPTION AND APPLICATION

2.1.1 GENERAL BIOSENSOR COMPONENTS AND CHARACTERISTICS

Leland Clark, known as the father of biosensors, developed the first true biosensor in 1956 for detection of oxygen [13]. His electrode for measuring oxygen is now known as the Clark electrode and numerous biosensors still utilize his design today. In 1962, Clark and Lyons [4] developed an electrode system to assist in continuous monitoring of blood oxygen, pH, and CO_2 levels during cardiovascular surgery and became the standard by which biosensors are made.

A biosensor or biological sensor is a device that translates the number of chemical or biological reactions to a proportionate electrical signal that can directly tell the concentration of an analyte in the reaction [13][14].

A biosensor consists of a few components, an analyte, a bioreceptor, and a transducer. There are additional external components such as electronics to process the transduced signal and a display to provide the information to the user/patient.

The analyte is the material of interest that needs to be detected. This could be a number of things to include lactate (used for sports sciences or clinical research), triglycerides, cholesterol, glycerol, alcohol, or glucose, just to name a few [13][14]. Glucose sensing is one potential target analyte and the operation will be discussed in Section 2.1.2.

The bioreceptor is the molecule or material that specifically identifies the target analyte [13]. Each analyte has its own associated bioreceptor. Some examples of bioreceptors are antibodies, DNA, enzymes, and aptamers. The interaction between analyte and bioreceptor produces different forms

of signals that can be analyzed in the form of light (optical), heat, charge, or simply a change in mass. The interaction process is known as biorecognition.

Lastly, the transducer is the component that converts the signal form (light, heat, charge, change of mass, etc.…) into a more useful form of energy [13]. Typically, the converted form of energy is an electrical signal or an optical signal that can be processed by the electronics and display as previously mentioned. This converted signal is usually proportional to the amount of analyte – bioreceptor interactions and subsequently means that this converted signal is proportional to the amount of the material of interest.

As previously mentioned, the electronics will take the converted signal, apply signal conditioning, amplification, and analog-to-digital conversions, and then quantified data will be sent to the display for the user/patient [13].

There are certain characteristics of all biosensors possess and the quality of the biosensor is determined by them. These characteristics are selectivity, stability, reproducibility, sensitivity, and linearity.

Selectivity of a biosensor is the capability to biorecognize a certain analyte amongst many other analytes [13]. A good example of this is to biorecognize only glucose in the blood or ISF when multiple other analytes are present. Selectivity is probably the most important characteristic. If a biosensor can't find the target analyte, there is no use in improving the other characteristics.

Stability of the biosensor is based on the vulnerability when exposed to ambient disturbances around the biosensor [13]. If the disturbances cause the measurements to drift or deviate, erroneous data will be shown which affects the accuracy and precision of the biosensor.

Reproducibility is the capability of the biosensor to reproduce the same output converted signal for multiple identical tests [13]. This provides a highly reliable and highly precise biosensor when there is minimal differential between each test. This can also show how robust the biosensor is if the reproducibility is consistent for many tests over a long period of time.

The sensitivity of the biosensor is related to the selectivity. The selectivity was whether or not an analyte could be detected whereas the sensitivity is the minimum amount of analyte that can be detected [13]. This characteristic is also vital because certain analytes require detection of small concentrations (ng/mL or fg/mL) to make determination of a medical course of action. In contrast, glucose sensing is typically in the mg/mL range meaning the sensitivity does not need to be as stringent.

The last characteristic is the linearity. Linearity is related to the accuracy of the biosensor by comparing the measured output versus a linear, straight line [13]. The concentration of analyte and the sensitivity of the biosensor determine the output signal. If the sensitivity is high, the resolution (smallest change required to induce a change in response) of the biosensor will also be high. A resolution that is better than the working range of the target analytes concentration is ideal. In other words, we need to be sensitive enough to detect the appropriate amount of concentration depending on the analyte to be detected.

Now that the basic properties of a biosensor are understood, it must be said that our biosensor array could be utilized for a multitude of different target analytes. Each target analyte has an associated enzyme that must be immobilized to properly detect said analyte. Each enzyme has its own effective lifetime ranging from days to weeks and with improved strategies of stabilizing the enzyme, that lifetime could potentially be increased below [14]. Some strategies include genetic

engineering methods, renewal of the inactivated enzymes, or incorporation of an external matrix such as nanofibers [14].

The ideal target analyte and enzyme for this work has not been determined but to give an example of the operation of an enzymatic biosensor, a glucose biosensor will be discussed in the next section.

2.1.2 GLUCOSE BIOSENSOR OPERATION

Biosensors used for monitoring glucose or glycaemia levels in diabetics typically utilize enzymes as the bioreceptors. These are known as enzymatic biosensors [16]. Enzymatic biosensors can still have different transduction methods such as electrochemical, optical, piezoelectric, or thermal. For glucose sensing in our work, the electrochemical transduction method is our choice due to its widespread use and is successful commercialized. The advantages of using electrochemical transduction include low cost and ease of fabrication.

Most commercialized glucose monitors utilize an enzyme known as glucose oxidase (GO_x) as the bioreceptor[16]. Interaction between glucose and oxygen with GO_x occurs on the working electrode of a three-electrode electrochemical biosensor. The chemical equation for interaction of these materials to form a readable electrical signal is derived and shown as follows:

$$\text{D-Glucose} + H_2O \xrightarrow{\text{Glucose Oxidase}} \text{D-Gluconic Acid} + H_2O_2 \quad (1)$$

The resulting chemical releases Gluconic acid and hydrogen peroxide (H_2O_2). The H_2O_2 then interacts with the biofluid (ISF or other biological fluid) and other electrodes to produce an electrical current flow proportional to the amount of H_2O_2 and subsequently the amount of glucose present.

Fang et al. [17] evaluated glucose sensors in 37°C serum (body temperature) to determine the lifetime with imitated in vivo conditions. By using polyaniline (PANI) nanofibers, they were able to improve immobilization of glucose oxidase and it was determined that the sensor was stable for 20 days with no degradation and remained at ~45% of its initial value after 44 days. This certainly provides a potential increase in functional lifetime when applied with our biosensor array.

2.2 NITROCELLULOSE HISTORY AND SOURCE

Many mechanisms for allowing biosensor activation could be utilized such as electrochemical dissolution of Au [9], expansion and contraction of hydrogels such as polyaniline (PANI) and poly(2-hydroxyethyl methacrylate (PHEMA) with voltage applied [18], or utilization of energetic polymers such as Peroxydone [19] and nitrocellulose. Each has its own advantages and disadvantages. We chose NC due to its relatively low decomposition temperature of ~200°C and its commercially availability which is commonly utilized in western blot testing for nucleic acid and protein detection. Also, it is highly formable in that with certain changes in parameters, the thickness or shape can be modified easily. Additionally, NC is a common membrane material used in biomedical applications which can be susceptible to biofouling but strategies might be possible to reduce this bacterial buildup [20]. In 2013, Yetisen et al. integrated nitrocellulose into their studies of paper-based microfluidics for POC devices to give an alternative option other than PDMS for real world products [22] and showed their potential use in medical devices. Therefore, this proved to be a good option for use as a decomposition mechanism and protective membrane to prevent premature biofouling of the biosensor array.

2.2.1 NITROCELLULOSE HISTORY

NC was discovered in 1832 by Henri Braconnot, a French chemist and pharmacist. He prepared a sample of NC by treating cotton with concentrated nitric acid (85%, v/v) [20]. This produced an

inflammable and unstable attempt resulting in a minimally nitrated cellulose (estimated at 4-5%). This was certainly the precursor to C.F. Schönbein's stable version in 1845. Schönbein was a German-Swiss chemist who came across a stable version by accident. The accident occurred when Schönbein spilled a mixture of nitric and sulfuric acids. After using a cotton apron to wipe up the mixture, he placed the apron near the oven. After the apron dried sufficiently, it spontaneously ignited and seemed to disappear. It was thought that this could be a cleaner and smokeless explosive to replace the common black gunpowder of the times. This violent reaction sparked many years in pursuit of making NC a replacement for black gunpowder. It was and continues to be one of the largest applications to date as an explosive and as a propellant [23].

Black gunpowder burns due to its ingredients undergoing chemical reactions whereas NC is inherently unstable and burns by decaying quickly with only hot gases released and virtually no smoke emitted. Additionally, the more the NC burns, the higher the gas pressure leading to its use as a wonderful propellant [24]. It is also commonly known as guncotton. NC or gun cotton did not come into use in gunpowder until the 1860s.

Some of the other well-known applications of NC have been employed by many industries. Some had success and some did not. In the late 19^{th} century into the early 20^{th} century it was actively used in lacquers, paints, and as a basis for fibrous and plastic materials [25]. The film and photography industry used thin NC films extensively to produce motion pictures. However, ignition of NC film stocks caused more than one fire to start with many casualties involved. This, for obvious reasons, led to more research into safer alternatives with cellulose triacetate being the material used by Eastman Kodak until the 1980s [26]. Even today, NC is utilized in common items such as nail polish, table tennis balls, and lacquers for wood finishing [27]. One other popular application for NC membranes is for a laboratory method known as a western blot. A western blot

is a method to detect certain protein molecules within a variety of proteins [28]. These same pre-cut membranes utilized for the western blot method will be the source of NC for this work.

2.2.2 NITROCELLULOSE SOURCE FOR THIS WORK

The source of NC for this work is from ThermoFisher Scientific as seen in Fig. 2.1 [29] which shows a manual flexing of the semi-rigid NC membranes to visualize the nature of the membrane. We used pre-cut sheets of NC originally designed for analytical techniques such as the western blot, dot-blot assays, and other protein methods. The pre-cut sheets are 7.9 cm x 10.5 cm with a 0.2 μm pore size. ThermoFisher Scientific [29] claims that each sheet is a pure, 100% NC membrane. The original intents and purposes of this membrane were not our goal. Rather, utilizing the pure, 100% NC in a different form was our intent. Knowing that NC was dissolvable in acetone [30], the intent was to take this dissolved acetone-NC mixture and determine whether or not a thinner membrane could be spin coated onto a surface. Then, by transferring this thin membrane to a separate structure to allow deposition of Au/Ti filaments, testing of NC could be implemented.

Figure 2.1 *NC membrane. 7.9 cm x 10.5 cm with 0.2 μm pore size. Manually flexed to visualize NC flexibility and semi-rigid behavior.*

2.3 CHEMICAL PROPERTIES OF NITROCELLULOSE

2.3.1 CHEMICAL REACTIONS TO FORM AND DECOMPOSE NITROCELLULOSE

Cellulose has different chemical derivatives according to [31] such as ester cellulose, ether cellulose, and cellulose nitrate (commonly called nitrocellulose). Each has its purpose and application but for this work, NC is the cellulose derivative of choice due to its unique chemical and thermal properties.

NC is an inorganic ester of cellulose and is the most commercially significant version of cellulose. Preparation of NC has been reviewed many times and different nitration techniques are utilized to make NC. However, NC is still commonly made by mixing cotton (or pulp wood in some applications), nitric acid, sulfuric acid, and water [32]. NC is formed by the esterification of the hydroxyl groups of cellulose with nitric acid along with sulfuric acid as a catalyst [10]. Other acids such as phosphoric acid or acetic acid can also be used as catalysts [10]. Historically, the chemical equation for interaction of these materials to form NC is derived and shown as follows:

$$\underset{\text{Cellulose}}{[C_6H_{10}O_5]_n} + \underset{\text{Nitric Acid}}{3HNO_3} \xrightarrow[H_2SO_4]{\text{Sulfuric Acid}} \underset{\text{Nitrocellulose}}{C_6H_7(NO_2)_nO_5} + \underset{\text{Water}}{3H_2O} \quad (2)$$

Cellulose and nitric acid are combined and by using sulfuric acid as the catalyst, a nitronium ion (NO_2^+) is formed which then bonds with cellulose to produce NC and an additional byproduct of water. The number of nitronium ions is a way to describe whether the cellulose nitrate (NC) is classified as cellulose trinitrate, dinitrate or mononitrate with $(NO_2)_3$, $(NO_2)_2$, (NO_2) representing the number of nitronium ions for each, respectively. In theory, during the esterification process, all three hydroxyl groups will be replaced by the nitronium ion producing cellulose trinitrate but

in practice most become cellulose dinitrate with ~1.8 to 2.8 [22] of the nitronium ions (NO_2^+) producing nitrate contents between 10.42% and 13.62%.

As previously mentioned, there are many variations of nitration techniques. Each nitration technique does produce a slightly different nitrate content [23]. However, the main difference between commercially available NC products is the nitrate content, solubility, and viscosity [33][34].

The thermal decomposition of cellulose trinitrate [20] occurs as described by the following equation:

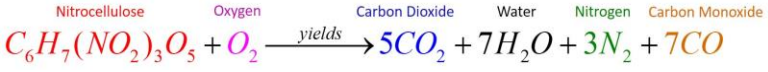

(3)

NC in the presence of oxygen and a heat source decomposes releasing the four byproducts shown in Eq. 3 which are carbon dioxide, water, nitrogen gas, and carbon monoxide.

2.3.2 NITRATE CONTENT OF NITROCELLULOSE

Nitrate content (also known as nitrogen content) is a chemical property that changes the way in which NC reacts. It is known that NC with a nitrate content of > 12.5% yields a material with a lower activation energy than a sample with a lower nitrate content**.** In other words, less energy is required to burn a higher nitrate content with lower decomposition temperature. The correlation between nitrate content and decomposition temperature is described in Section 2.4.1. The opposite is true of NC with nitrate content of < 12.5% in which it still possesses flammable attributes but not as explosive [20]. Therefore, it requires more energy (higher activation energy) to cause decomposition.

The different nitration techniques are not described here but Saunders and Taylor [23] describe in detail the techniques and it can be seen that each technique would be useful in different applications. NC with the highest possible nitrate content is classified as a fully nitrated cellulose, or cellulose trinitrate, and has nitrate content of 14.15%. The next lowest classified NC is cellulose dinitrate with nitrate content of 11.11%. The lowermost classified NC is cellulose mononitrate with nitrate content of 6.76%. Each of these classifications, cellulose trinitrate, cellulose dinitrate, and cellulose mononitrate are the typical method of reporting in papers and articles [23]. Each of these classifications come from determining the percentage of nitrogen versus the entire molecular weight of the NC. For cellulose mononitrate, nitrogen makes up 6.76% of the entire molecular weight and the reason for the lower percentage is the presence of only one nitronium ion (NO_2^+). The other two common nitrate contents, 11.11% and 14.15% represent the presence of two (NO_2^+) and three (NO_2^+), respectively. Based on the chemical reaction shown in Eq. 3, 14.15% would be the nitrate content.

As previously mentioned, there are different nitration techniques which can produce different nitrate contents. Briefly, the nitrate content can be modified by a few factors such as the strength of the acid, the source of the cellulose, the temperature, and also simply by changing the acid to cellulose ratio. By controlling these conditions, the desirable nitrate content can be achieved.

Given the three classifications described above and based off knowledge of when NC becomes explosive described earlier, we can roughly determine which classification our NC is by burning a sheet and visually determining the classification. Approximately 12.5% is the cutoff which means that above this percentage is conclusively either cellulose dinitrate or cellulose trinitrate. If the sheet explodes, then it is safe to say it is either of these two classifications. However, if the sheet is only flammable and not explosive, then the nitrate content is below 12.5% which excludes

the cellulose trinitrate classification. This brings in the possibility of the material being cellulose mononitrate. But, it is known that cellulose mononitrate is almost non-useful and while not completely non-flammable, it produces a far less violent burning than cellulose dinitrate.

After performing a burn test, we can safely say that our material is not cellulose trinitrate. It was still violent enough of a reaction to conclude that our nitrate content was moderately high. It was not explosive but the material quickly decomposed instead of slowly burning. Most likely, our material is cellulose dinitrate with a nitrate content <12.5%. This knowledge will be helpful in understanding the solubility and thermal properties discussed in later sections.

2.3.3 SOLUBILITY OF VARYING NITRATE CONTENTS

Any particular NC sample has its own unique nitrate content level. For this work, NC was dissolved in acetone based on work done by Wilson and Miles in 1934 [35]. The observed response of solubility (purely from visual inspection) shows that each sample dissolves in acetone very similarly. Our NC is outsourced and it is expected that each sample is close to identical.

As explained in [23], solubility of the sample is dependent on the nitrate content. Given that our NC should be close to identical, nitrate contents should be similar as well. Therefore, by using the graph shown in Fig. 2.2 [23], a comparison of our material and a mixture of NC and ether/alcohol solution can be made. Even though the solvent is slightly different than ours, the principle is the same.

It can be seen from Fig. 2.2 that there is a significant increase in solubility of the material with nitrogen content just below 9% and then a sharp decrease just below 13% [23]. This graph illustrates that cellulose mononitrate and cellulose trinitrate will have low solubility making it harder to dissolve whereas cellulose dinitrate, which could be considered in the range of 9 to 13%

of nitrogen content, has a higher solubility. This information clarifies and further solidifies our assumption that NC used in this work is most likely cellulose dinitrate. Our NC has sufficient solubility in acetone to proceed with further testing.

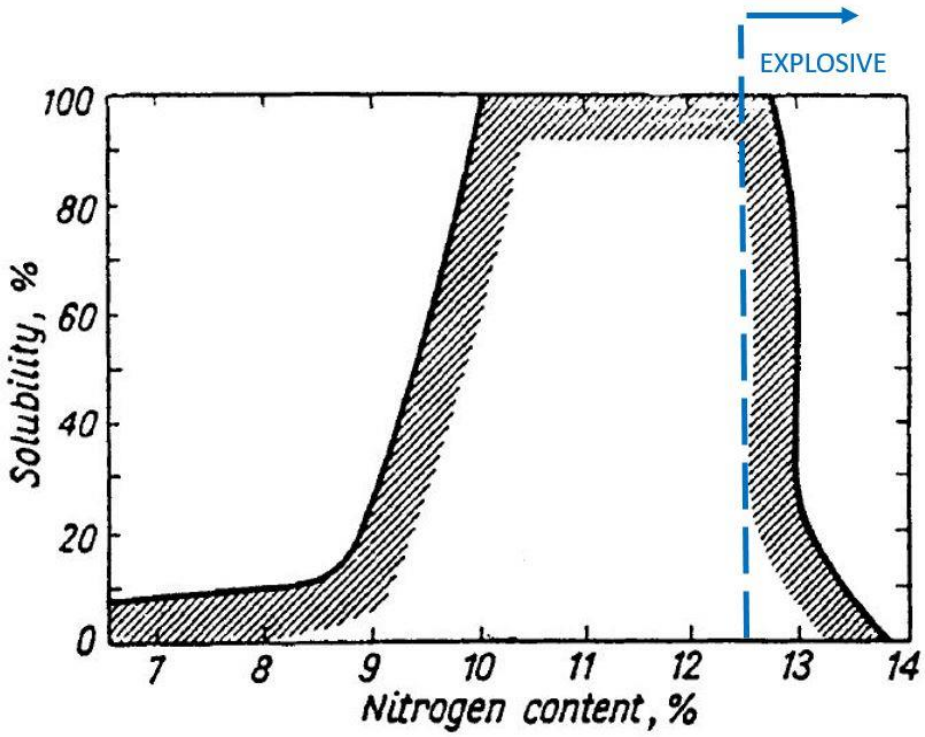

Figure 2.2 *Solubility of NC in Ether/Alcohol solution versus nitrogen content (also known as nitrate content) of sample* [18]. *Explosive region shown as nitrogen content greater than 12.5%.*

2.4 THERMAL PROPERTIES OF NITROCELLULOSE

NC is a dangerous substance that has flammable and explosive potential. As previously mentioned, NC is utilized as a propellant and the nitrate content determines NC's propensity to be explosive or just flammable. For modern gunpowders, a higher percentage of nitrate content produces a faster muzzle velocity of a bullet by using a NC with nitrate content >12.5% to achieve an explosion [20][36]. There is still some explosiveness at moderately nitrated cellulose of <12.5% but it is far less violent [36]. Changing nitrate content and changing heating rate of NC has an effect on the

thermal decomposition temperature. These two effects will be discussed in the Thermal Properties section.

2.4.1 EFFECT OF NITRATE CONTENT ON DECOMPOSITION

As above-written, the nitrate content determines the explosiveness and flammability. An understanding of how the nitrate content affects the decomposition of NC must also be understood. To determine how NC decomposition is affected, a few thermoanalytical techniques were applied.

The first is Differential Scanning Calorimetry (DSC). DSC is a technique in which heat flux (power) to a sample is characterized with respect to temperature as the temperature is varied. In other words, it is the difference in the amount of heat required to increase the temperature of a sample and reference as a function of temperature [37]. If results show a positive change in the heat flux, this is an exothermic reaction of the sample. Conversely, if results show a negative change, this is an endothermic reaction of the sample.

Differential Thermal Analysis (DTA) is a technique for identifying and quantitatively analyzing the chemical composition of a substances by observing thermal behaviors as a sample is heated. To rephrase it, a material and reference undergo identical thermal cycles while recording any temperature difference between them. This will again show a heat flux versus temperature that shows the similar exothermic/endothermic reactions as DSC. DTA can be combined with the next technique known as Thermogravimetric Analysis (TGA) to get TG/DTA [38].

TGA is a technique in which the mass of a sample is examined over time as temperature changes. As previously stated, this can be combined with DTA to get characterization of a materials exothermic or endothermic behavior and the sample mass as a function of temperature [39].

Pourmortazavi et al. (2009) [40] diligently analyzed NC with the above-mentioned techniques. Their resultant data shed light on the effect of nitrate content on the decomposition of NC. The results shown in Fig. 2.4 are for the NC sample with a 13.9% nitrogen content with weight of 3 mg. The analytical technique employed for Fig. 2.3 was the TG/DTA combination. The DTA results (Blue curve in Fig. 2.3) show that heat flow is positive and increases rapidly starting just below 200°C with a peak at approximately 201°C implying an exothermic reaction. Likewise, the TGA results (Red curve in Fig. 2.3) show a rapid decrease in mass as exothermic behavior occurs. In short, 201°C is the temperature at which thermal decomposition happens. Characterization of thermal decomposition temperature at a specific nitrate content is valuable. Determination of this decomposition temperature will help define the minimum threshold that must be achieved to begin decomposition of NC.

In Fig. 2.4, the effect of nitrate content on thermal decomposition temperature is shown. There are four (4) different samples, NC1, NC2, NC3, and NC4 with nitrate contents of 13.9%, 13.5%, 12.9%, and 12.5%, respectively. This graph shows the DSC analytical technique results and the most important point is that decomposition temperature changes with nitrate content. NC1 is similar to results in Fig. 2.4 and NC2, NC3, and NC4 exhibit an increased shift in decomposition temperature as nitrate content decreases. This information gives useful understanding of what is to be expected in this work. However, the nitrate content is not the only factor that can change the decomposition temperature. The rate of temperature or heating rate during the analysis can also alter the decomposition temperature.

The effect of heating rate on decomposition temperature is shown in Fig. 2.5 and once again DSC was the analytical technique employed. Decomposition temperature was determined at four (4) heating rates, 5°C/min, 10°C/min, 15°C/min, and 20°C/min. There is a clear shift in the

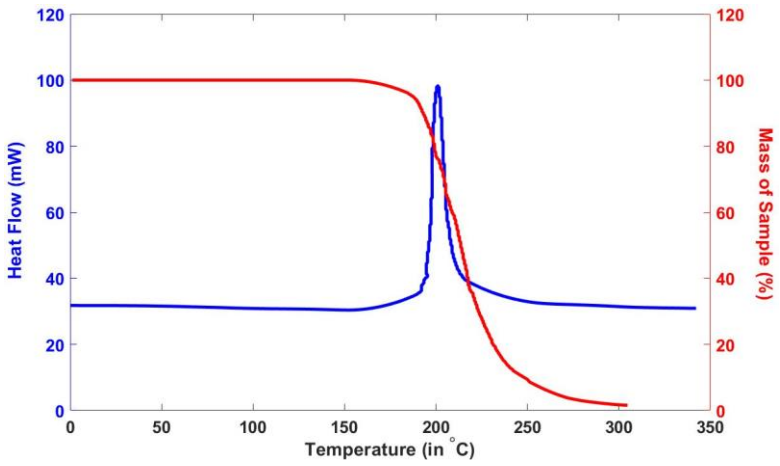

Figure 2.3 *NC with 13.9% nitrate content. DTA Curve (Blue Curve): Heat flow is changing positively showing sharp exothermic behavior at approximately 201°C. TGA Curve (Red Curve): Mass of Sample (in %) showing rapid decrease in mass as exothermic behavior occurs. Customized from [40]*

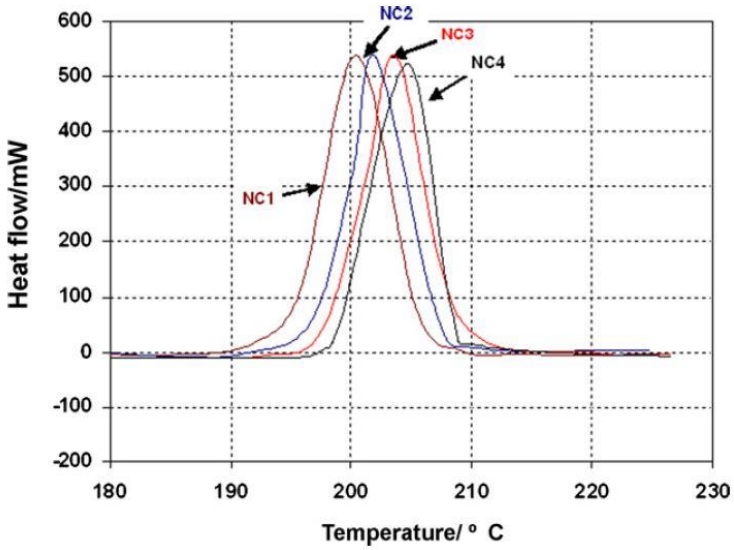

Figure 2.4 *Effect of nitrate content on the DSC results of NC. NC1 – 13.9%; NC2 – 13.5%; NC3 – 12.9%; NC4 – 12.5%. Sample mass of 3 mg in a Helium atmosphere [40].*

decomposition temperature with different heating rates. Effect of heating rate is inverse to the response of change in nitrate content. As heating rate increases, the decomposition temperature

will increase. A higher nitrate content would decrease the decomposition temperature, and hence the inverse relation.

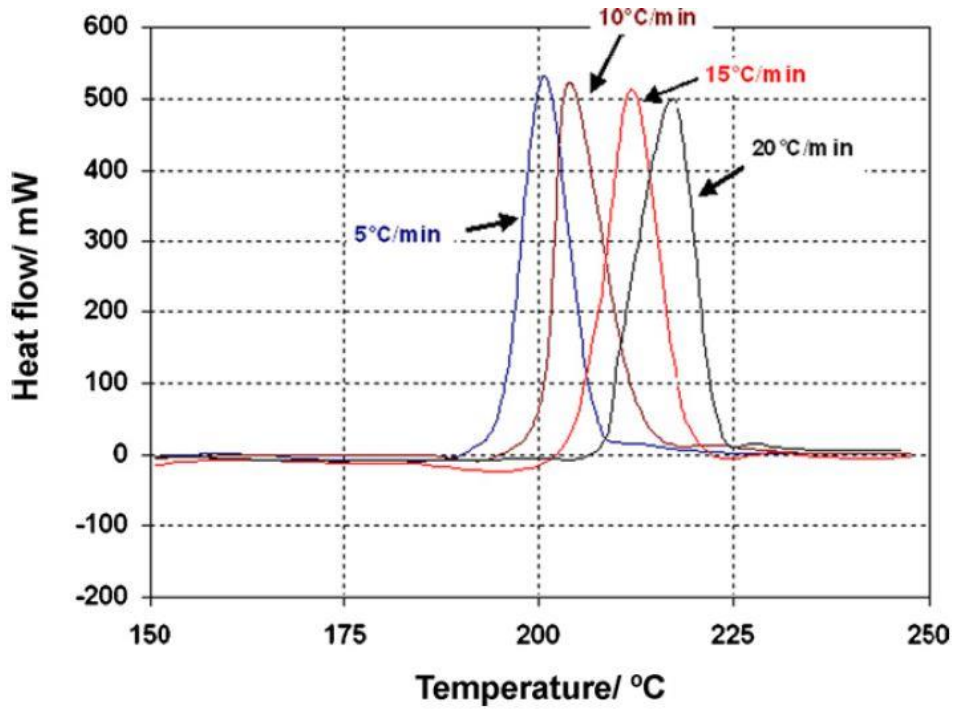

Figure 2.5 *Effect of heating rate on the DSC results of NC with 13.9% nitrate content. Sample mass of 3 mg in a Helium atmosphere [40].*

For this work, the impact of change in heating rate will prove to be more detrimental on the results than if nitrate content is altered. An increase in nitrate content of 1.4% only results in a 5°C reduction in decomposition temperature. Meanwhile, with only a 5°C/min change in heating rate, a 5 – 6°C rise in decomposition temperature occurs. To change the nitrate content from 13.9% to the maximum of just over 14% to get true cellulose trinitrate will result in minimal decrease in decomposition temperature. This improvement will be quickly negated by changing the heating rate only slightly. However, it is shown that the nitrate content greatly affects thermal stability [40].

Regardless of the nitrate content present in our work, the method of increasing local temperature to achieve thermal decomposition of NC is to apply a current through an Au/Ti filament deposited atop the NC. The required amount of current or energy to apply is discussed in Section 2.5. Sufficient energy applied to a thin-film of metal will increase the temperature of the filament and this increase in the local temperature will be significantly higher than the decomposition temperature previously discussed. As previously mentioned, the more rapid rate of increase in temperature will increase the decomposition temperature of NC but the local temperature due to the Au/Ti filament Joule heating will be significantly higher.

We know that the evaporation temperature of Au is around 1400°C [41] when utilized in thermal evaporation processes and our expectation is that Au will explosively decompose implying the local temperature of NC will be sufficiently high to achieve thermal decomposition.

2.5 EXPLOSIVE DECOMPOSITION OF METAL THIN-FILMS

Research of the behavior of thin metal films and wires under exposure to varied current densities was performed to determine the appropriate current density that will lead to explosive decomposition of our thin-film Au/Ti filaments. The following research refers to their work as either explosion or explosive decomposition based on the type of research performed. It appears that the larger the current density, the more likely it is to be called explosion. For our work, we will refer to it as explosive decomposition.

The behavior of exploding Gold (Au) wires was investigated by Tucker [42] and was determined that at current densities of 0.25×10^8 to 3.26×10^8 A/cm^2 for a 1-mm diameter, 0.1-in length Au (99.99%) wire, the wire undergoes metal heating and phase transformations in sub-μs times. Using a current pulse from a square-wave generator of 3 μs duration with maximum of 2000 A,

vaporization was achieved in the 1 – 10 μs range depending on the current density. This shows that gold wires exploded by current density have electrical resistance and total energy input as functions of current density.

Karimkhodzhaev and Martynyuk [43] investigated electrical explosion of Copper (Cu) (99.99%) and Au (99.99%) wire specimens of 0.3-mm diameter, 50-mm length in air. Using a 100 μF capacitor charged to 3 kV, a powerful current pulse was discharged through the wires to achieve explosion within a few μs.

Aguilar et al. [44] studied the effect of electrical current (DC) on Au thin films. Their test involved deposition of a 3 – 4 μm thick gold film on a 7059 Corning glass substrate and then determined the film roughness. Next, they applied a relatively low current density of 0.25×10^3 and 0.25×10^4 A/cm^2 corresponding to currents of 0.1 and 1 A, respectively. Then, by testing for specified times, it was determined that the surface of the gold film went from rough to smooth grains when current was applied up to 2 weeks due to electromigration. The larger of the current densities, 0.25×10^4 A/cm^2, was applied continuously for 2 wks before failure of the film occurred.

M.K Marakhtanov and A.M Marakhtanov [45] applied different current densities gradually to different cold thin metal films to characterize the processes that take place in the metal. These processes include the thermoelectronic valve phenomenon, the heat wave, the deformation wave, and then explosive decomposition of the metal. Their testing involved Aluminum (Al), Copper (Cu), Nickel (Ni), Titanium (Ti), Tin (Sn), and Tungsten (W) thin films of thicknesses ranging from 6.5 to 49 nm. A DC power supply with current and voltage ranges of 0 – 8 A and 0 – 600 V, respectively, was used. The current was raised gradually over 20 – 40 s until explosion occurred. The critical current densities for Al, Cu, Ni, Ti, Sn, and W are 8.04×10^5, 7.29×10^5, 7.41×10^5,

3.78 x 10^5, 1.32 x 10^5, and 1.43 x 10^5 A/cm^2, respectively. Once the appropriate current density was reached, the film explodes over a time period of 1 – 8 μs. An adverse effect of their test was deformation in the substrate due to the shock wave of the electrical explosion.

Li et al. [46] designed and tested a drug delivery MEMS device to release multiple substances in vivo. The design was based on work done by Santini, Cima, and Langer [9] on a controlled release microchip. By using anodes and cathodes of 0.3 μm thick gold, the membrane was released or removed via electrochemical activity. A square wave generator utilized with frequency of 1 Hz from 0 – 1.1 V for 20 mins was required to remove the anode over a reservoir for flow of substances.

Lastly, Kim et al. [47] utilized an RLC initiation circuit to burst thin film metallic bridges for design of electrical initiation devices in explosive charges. Their testing involved Al and Cu but mentioned Au and Silver (Ag) as potential bridge materials as well. The thicknesses varied from 30 – 170 μm in testing of how quickly the bridge would burst versus thickness. The burst time ranged from 0.25 – 3.75 μs when a charging voltage of 40kV resulting in current density of 0.54 x 10^8 A/cm^2 applied. Their paper additionally tested bridge size, charging voltage, and material versus bridge burst time. They numerically modeled the ideal conditions for application in explosive devices and concluded that the copper bridges were more suitable due to better initiation performance.

3 PROCESS DEVELOPMENT AND FABRICATION

The goal for this work is to establish an area for biofluid collection and a mechanism to allow biofluids to interact with a biosensor. The fabrication of the biosensor is not included in this work due to the potential for numerous types of biosensors to be used. A brief explanation of how biosensors work and one example, glucose biosensing, were described in Sections 2.1.1 and 2.1.2, respectively. An exploded view of the single biosensor unit described in section 1 can be seen in Fig. 3.1. Fabrication of the PDMS well structures, thin-film NC membrane and deposition of a thin-film Au/Ti filament will be discussed in this section. In addition to the description of fabrication methods, a brief explanation of the design requirements will be discussed which aids in determination of how small or large our design will become.

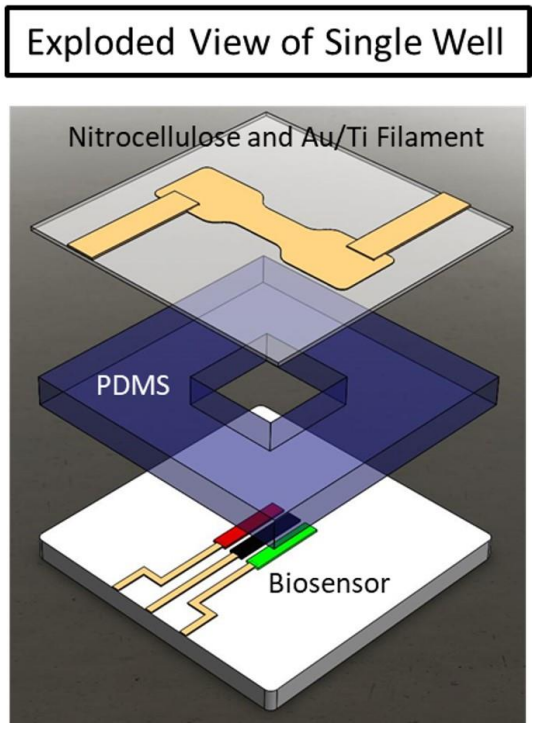

Figure 3.1 *Proposed solution consisting of three main components, a substrate with a biosensor (not discussed in fabrication), a PDMS well structure housing, and a decomposition mechanism consisting of a thin-film nitrocellulose membrane and thin-film Au/Ti filament.*

3.1 DESIGN REQUIREMENTS

Requirements for long term commercial application using NC as controlling mechanism in an on-demand biosensing system are straight-forward.

The first requirement is the system must be compact enough to cover minimal area in or on a patients' body. This is accounted for by making each system comparable to a current commercial market CGM device. Each system comprises an array of biosensors that can be individually described by three components, a non-biofouled biosensor awaiting activation, a PDMS mold that forms a well for bio-fluid collection, and a NC membrane enclosing the well with an Au/Ti filament on top of the membrane to decompose NC. Each sub-system (Biosensor, PDMS well, and NC membrane with Au/Ti filament) takes up an approximately 4 mm^2 which, if scaled correctly, can be reduced to adjust for smaller applications. Putting these structures close enough to each other will also help minimize the total area.

The electrical power requirements are an additional concern. If the overall system must be small, then the batteries used would need to be small watch batteries with voltage ranging from 1.5 – 4.5 V. Using small watch batteries requires that the amount of power and current be minimized. In order to have a long lifetime, with a watch battery having a rating of 100 – 200 mAh, the current must be short pulses to maximize the full potential of the battery. A rating of 100 mAh means that the battery can output 100 mA for 1 hour continuously before it is no longer useful. In order for this to be commercialized, the lifetime of these batteries must be maximized.

Given a moderate current of 0.5 A and assuming a 50 ms opening time, only 6.9 µAh will be required to open each well. Assuming an array of 10 biosensors and assuming each biosensor will be functional for 14 days (based on [6]), we can reasonably improve the overall functional lifetime to 140 days. This is 50 days longer than the current state-of-the-art Eversense CGM (US Version)

[8]. This is does not take into consideration stability of the enzymes used or the long-term effects of NC exposure to biofluids. These must be addressed in future work.

3.2 FABRICATION OF PDMS WELL STRUCTURES

The foundation of the project that forms a path for controllable access of the biosensor to interstitial fluid (ISF) is the PDMS well structures. To fabricate the well structure, a mold must be made. Of course, there must be redundancy and therefore, a mold with multiple well structures were made. There are many methods and materials that can be exploited to fabricate these well structures. If it was a non-flexible application, a piece of steel or aluminum could be milled to the precise dimensions required. Even a 3D printed array of well structures could be made. For flexible applications, especially for biomedical and microfluidics, Polydimethylsiloxane (PDMS) is a preferable material [48].

Given a master mold, a PDMS casting that contains well structures can be performed. To make the mold, a small 50 cm x 50 cm x 0.8 cm (length x width x depth) aluminum plate was machined to exact dimensions required for this project. This mold can be seen in Fig. 3.2 and also shows pre-cured PDMS casted into the mold. The exact procedure for producing an appropriate amount of PDMS to cast into the aluminum mold is described in [49]. For this work, 3 g of base and 0.3 g of curing agent (Dow Corning Sylgard 184 Silicone Elastomer) are used as the 10:1 base to curing agent ratio. When this ratio is utilized in the master mold, ~1.5 mm depth well structures are produced.

The curing process can occur in a few different ways. For the PDMS used, the datasheet [49] gives different cure times at differing temperatures. Table 1 shows the cure times versus temperatures for PDMS and also temperature and time reported by Xia and Whitesides [48], which were utilized

for this project based on another authors work. The typical time and temperature employed for this work was 6 hours at 80°C. This allowed for highly controllable and reproducible results while minimizing the manufacturing time.

Table 1. Sylgard 184 Silicone Elastomer Cure Temperatures and Times

Cure Temperature	Cure Time	Datasheet/Paper
25°C	48 hours	Sylgard 184 Silicone Elastomer [49]
100°C	35 minutes	Sylgard 184 Silicone Elastomer [49]
125°C	20 minutes	Sylgard 184 Silicone Elastomer [49]
150°C	10 minutes	Sylgard 184 Silicone Elastomer [49]
80°C	6 hours	Used as a guide for this work [48]
60°C	12 hours	Used as a guide for this work [48]

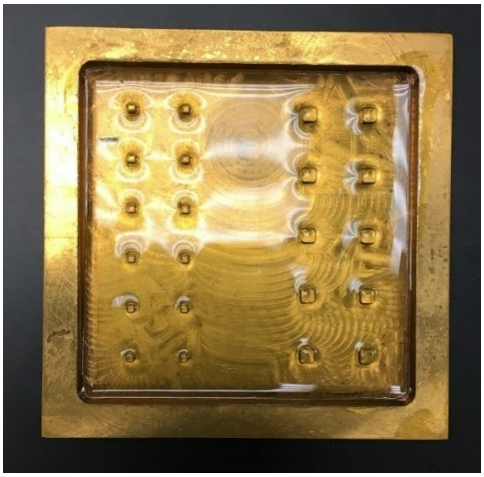

Figure 3.2 *Aluminum plate (50 cm x 50 cm x 0.8 cm) machined to create a mold for casting PDMS well structures. Titanium Nitride (TiN) has been deposited on the surface of the aluminum via Atomic Layer Deposition (ALD) to create a low adhesion surface to assist the removal of cured PDMS Well structures. Using 3 g of PDMS base and 0.3 g of PDMS curing agent produces well structures with a depth of 1.5 mm.*

3.3 FABRICATING NITROCELLULOSE MEMBRANES OVER PDMS

To produce a controllable monitoring system, a method of accessing the previously fabricated PDMS well structures as outlined in Section 3.1 must be addressed. This method is realized by a thin, destroyable membrane made of NC. A NC membrane is fabricated by a specific procedure established to convert a thick, semi-rigid NC sheet (ThermoFisher Scientific) as previously described in Section 1.3 into a thinner, more pliable NC membrane. After the membrane has been spin-coated, a gluing process is used to attach the thin NC membrane to the previously fabricated PDMS well structures. This section will outline the procedure to spin-coat a thin NC membrane and describe the transfer process to PDMS well structures. The following procedure is a generalized set of steps and any alterations from this procedure will give different results than expected.

3.3.1 SPIN-COAT PROCEDURE FOR NITROCELLULOSE MEMBRANES

A visual representation of the NC spin-coat process can be seen in Fig. 3.3 and a thin-film of NC on a substrate can be seen in Fig. 3.4. Starting with a Pt covered Sapphire substrate, NC is applied to the substrate as described above. Then, NC is spin-coated at a predetermined speed for the thickness required. After sufficient drying time has elapsed, measurement of the thickness can occur and transfer of NC can be performed. For a more detailed step-by-step spin-coat procedure, see Appendix A.

Coating of substrate with a low adhesion metal such as Platinum (Pt) is essential for transfer of a thin NC membrane to PDMS well structures. To allow for easy removal of the NC membrane from the substrate, Pt was electrochemically deposited on to a Si or Sapphire substrate. To establish good contact of Pt to either a Si or Sapphire substrate, a thin layer of Titanium (Ti), which acts as an adhesion layer, and Gold (Au), which acts as the adhesion layer for Pt, are

deposited via Electron-Beam Physical Vapor Deposition and Thermal Physical Vapor Deposition, respectively.

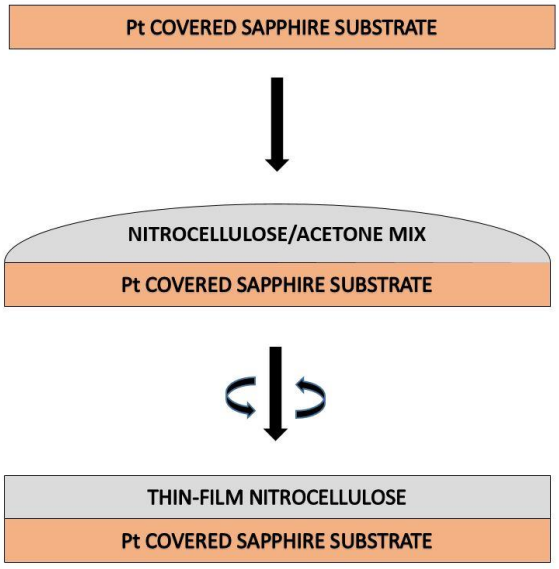

Figure 3.3 *Spin-coating of NC on Pt covered substrate.*

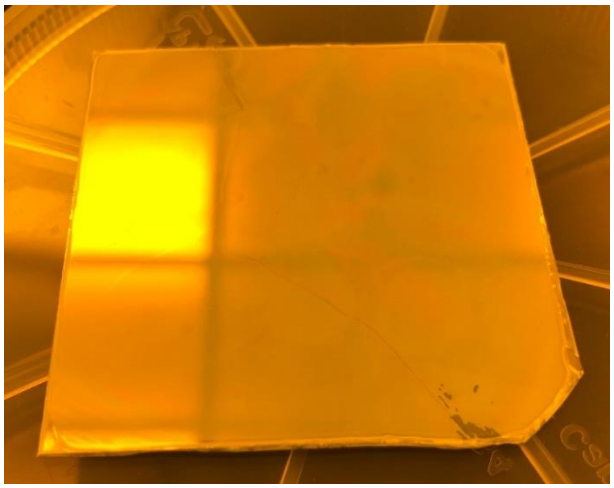

Figure 3.4 *Representative image of NC spin-coated on Pt covered substrate.*

After the physical depositions, thermal annealing is performed before electrochemical deposition of Pt. Thermal annealing is done for 10 mins at 350°C under N_2 is performed to reduce the stress in the Au film before electrochemical deposition of Pt.

To transfer the previously spin-coated membrane to the PDMS well structures, a unique transfer process was required. NC could not be directly spin-coated on to PDMS well structures as the NC would then enter the well structures which is undesirable. The quickest and easiest method was to "glue" them together. By utilizing the procedure in [49] that describes how to mix a PDMS sample, a "glue" is fabricated. The procedure in Section 3.3.3 describes the transfer of a previously spin-coated NC membrane to PDMS Well Structures with a PDMS "glue".

3.3.2 SPIN CURVES

NC dissolved in acetone allows us to take a previously semi-rigid sheet (ThermoFisher Scientific) and make thinner, more usable membranes for our application. To establish control over thickness of each membrane, a spin curve had to be established.

Spin curves are common among photoresist datasheets. Different applications require different thicknesses of photoresists. Each photoresist spin curve typically shows a certain behavior between the speed of the spin-coater and thickness of the resultant photoresist layer. As spin speed of the spin-coater increases, thickness of the photoresist decreases. Typically, at low spin speeds (500 – 2000 RPM) the thickness changes rapidly as the spin speed is slightly increased. Then, as speed increases further, the thickness reaches a saturation thickness in which increasing the speed will result in minimal change of thickness.

Additionally, each photoresist has a different viscosity which is measured in centiStokes or cSt or in SI Units of mm^2/sec. Viscosity is a measure of how resistive a material is to flow at a given rate.

If a material has a certain viscosity, it will produce a unique thickness range dependent on that viscosity. A high-resolution photoresist such as SPR 3012 [50] has a lower viscosity (24.3 cSt) compared to a lower resolution photoresist such as SU-8 2100 [51] with a higher viscosity [38] (12900 cSt). A medium-resolution photoresist such as AZ 4620 [52] has a viscosity of 536 cSt. Through interpretation of the respective datasheets, it can be shown that the higher the viscosity, the thicker the resulting layer on a substrate. This is evidenced from the thickness ranges of each photoresist. SPR 3012 has a range of 0.8 – 1.7 μm whereas SU-8 2050 has a range of 40 – 170 μm. Just as a comparison, the viscosity of water is 1 cSt.

By understanding that thickness of our membranes can depend on both spin speed and viscosity, we can establish spin curves that should give repeatable results. Thickness of all membranes spin-coated on substrates verified by means of a Veeco DEKTAK 150 Surface Profilometer. The physical location was typically near the edge of the wafer in a location that would not impede the Au/Ti deposition or usefulness of the NC membrane. One example of measurement location can be seen in Fig. 3.5 by a black oval. A portion of NC membrane was peeled off by tweezers to allow for measurement.

An example of the DEKTAK Profilometer graphical output can be seen in Fig. 3.6 and a SEM image for visual confirmation can be seen in Fig. 3.7.

The spin rate versus thickness graph as seen from Fig. 3.8 demonstrates a multitude of information. There is a note to make about the samples. As discussed later in this part, the more the material or the lower the amount of acetone, the higher the solid fraction of NC in acetone. The solid fraction of NC in acetone is determined by the ratio of weight of NC in grams to volume of acetone in mL.

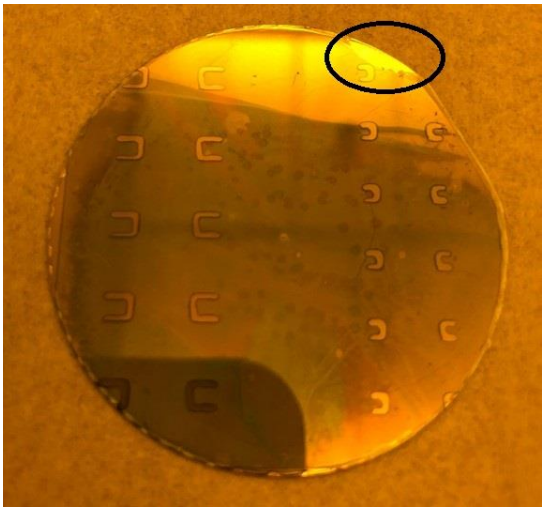

Figure 3.5 20 *nm Titanium (Ti) as an adhesion layer with* ***80*** *nm of Gold (Au) acting as a filament deposited directly on NC covered substrate. NC thicknesses of* ***1.16, 1.89, and 2.52 µm*** *as measured by profilometer at location in black oval.*

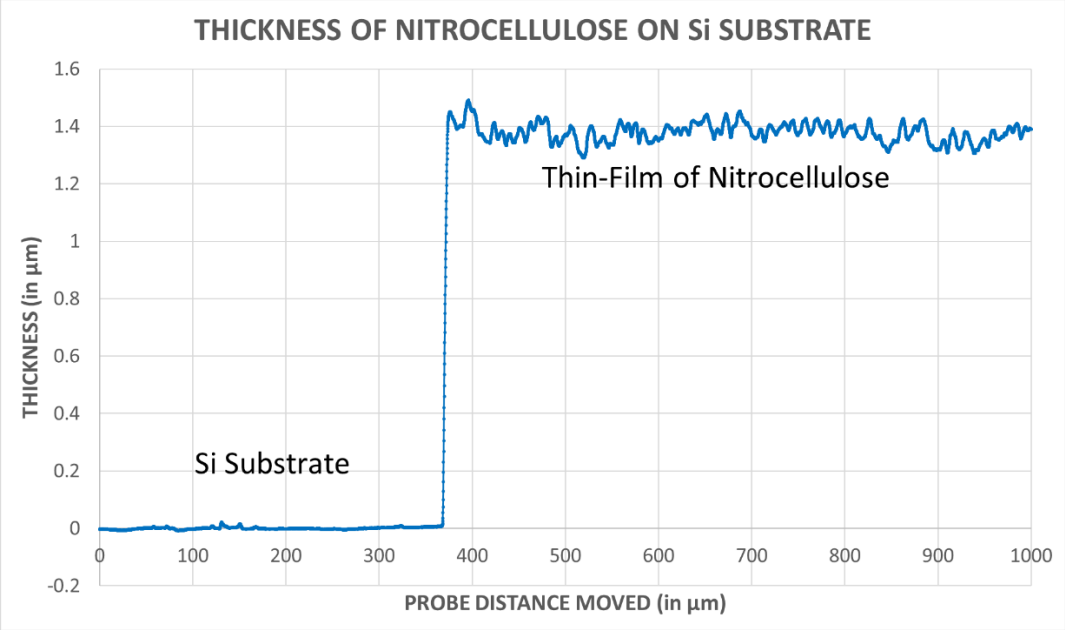

Figure 3.6 *Example of Dektak Profilometer graph output showing probe distance versus thickness. Left side of graph shows Si Substrate and a clear transition can be seen to the thin-film of NC on the right side of the graph. In this case, average thickness was calculated from all points 400 µm to 1000 µm. Average thickness was* ***1.38 µm****.*

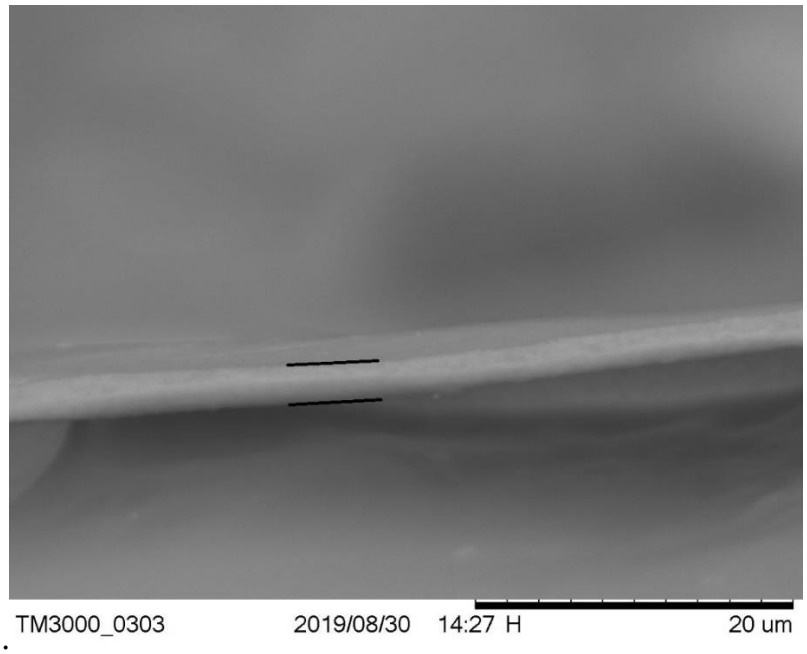

Figure 3.7 *SEM image for visual confirmation of NC thickness*

This ratio is known as weight to volume (W/V) and, for this work, will reported as such. The W/V ratio is not 100% analogous to viscosity but similar in nature. When a material has a higher viscosity, the W/V ratio tends to be higher as well. We determined that by controlling the volume, the NC/Acetone mixture became more viscous and was the easiest variable to modify when mixing.

In order of highest viscosity to lowest viscosity would be as follows in Fig. 5.4:

1. FULL SHEET OF NC DISSOLVED IN 10 mL ACETONE – BLUE
   -Produced an Average W/V ratio of 0.0555 g/mL

2. FULL SHEET OF NC DISSOLVED IN 15 mL ACETONE – RED
   -Produced an Average W/V ratio of 0.0373 g/mL

3. FULL SHEET OF NC DISSOLVED IN 20 mL ACETONE – GREEN
   -Produced an Average W/V ratio of 0.0280 g/mL

4. HALF SHEET OF NC DISSOLVED IN 20 mL ACETONE – MAGENTA
   -Produced an Average W/V ratio of 0.0139 g/mL

First, thickness variation with changing spin rate was tested while maintaining the W/V ratio constant. Each color in the figure represents a different W/V ratio by adjusting either amount of NC or amount of acetone. A curve can be seen for each W/V ratio.

Then, thickness variation with changing W/V ratio was tested while maintaining spin rate constant. Based on order of highest to lowest W/V ratio shown in Fig. 3.8, it can be seen that the higher the W/V ratio, the thicker the NC membrane.

In summary, overlay of the four curves as a comparison shows that the thickness does indeed change with both spin rate and solid fraction of NC in acetone.

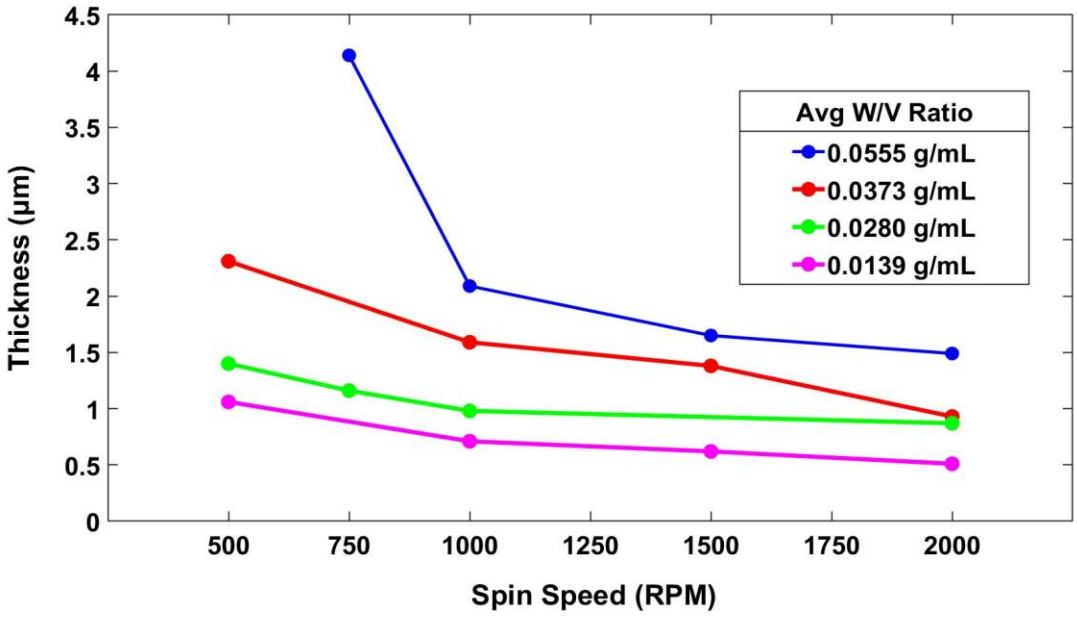

Figure 3.8 *Nitrocellulose Spin Curves for different W/V ratios*

Specific, repeatable instructions to spin-coat NC on any given substrate must be established to perform proper systematic testing. Therefore, the parameters and instructions described in Appendix A can be utilized to achieve NC membrane thicknesses comparable to the thicknesses

on the aforementioned spin curves. The spin-coater used for applying the NC membranes to substrates is a Laurel Technologies Model WS-650 MZ.

3.3.3 TRANSFER OF NITROCELLULOSE MEMBRANES TO WELLS

Transfer of thin-film NC membranes from a low-adhesion substrate to PDMS well structures is necessary to establish the barrier against biofluids. The procedure for this transfer is described in Appendix B and a visual representation of the transfer process is shown in Fig. 3.9.

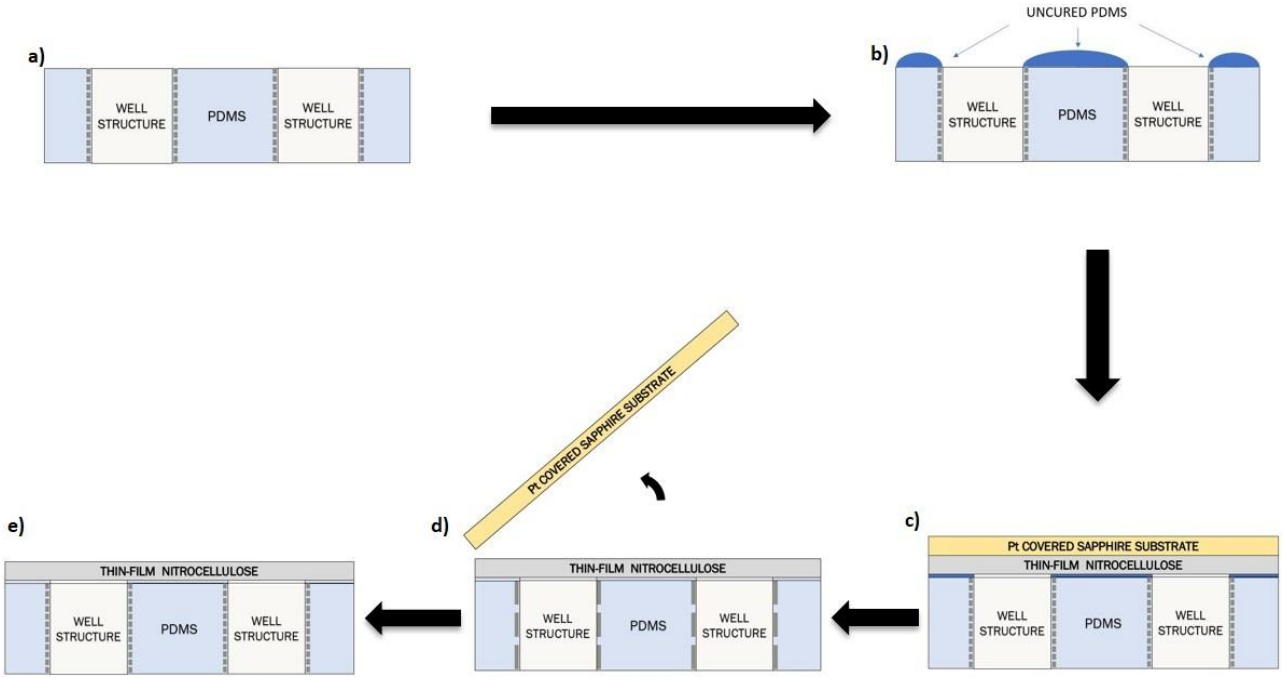

Figure 3.9 *NC transfer process from Pt covered Sapphire substrate to PDMS well structures.* ***a)*** *Starting with PDMS well structures* ***b)*** *a PDMS "glue" is applied.* ***c)*** *Then, the previously spin-coated NC to Pt covered Sapphire substrate is bonded to the PDMS well structures.* ***d)*** *After sufficient drying time has elapsed per Table 1, the Pt covered Sapphire substrate is removed,* ***e)*** *leaving a thin-film nitrocellulose membrane attached to one side of the PDMS well structures.*

3.4 DEPOSITION OF Au/Ti ON NC – 3D PRINTED SHADOWMASK

In order to test NC, filaments must be deposited on to NC membranes in a specific pattern. As will be described further in Section 3.5, deposition with standard photolithography will not suffice. Therefore, a 3D printed shadowmask was made to perform this task. Fig. 3.10 shows the AutoCAD 3D rendering of the shadowmask employed for this work. Autodesk Inventor Professional 2019 was used to render all iterations of shadowmasks. Two of the resultant shadowmasks used in this work are shown in Fig. 3.11.

After the shadowmask was built and NC transferred to PDMS well structures, evaporation or deposition of Ti and Au was performed. 20 nm thick Ti was applied as an adhesion layer between NC and the 80 nm thick Au filament layer. A cross-sectional view of the evaporator holder, NC/PDMS well structures, and shadowmask are shown in Fig. 3.12.

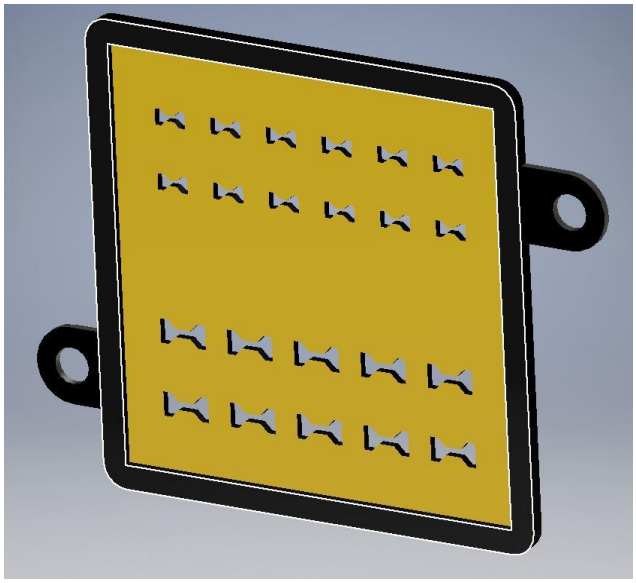

Figure 3.10 *3D rendering in Autodesk Inventor of shadowmask utilized for deposition of Au/Ti on NC. Tabs are used for mounting to evaporator holder.*

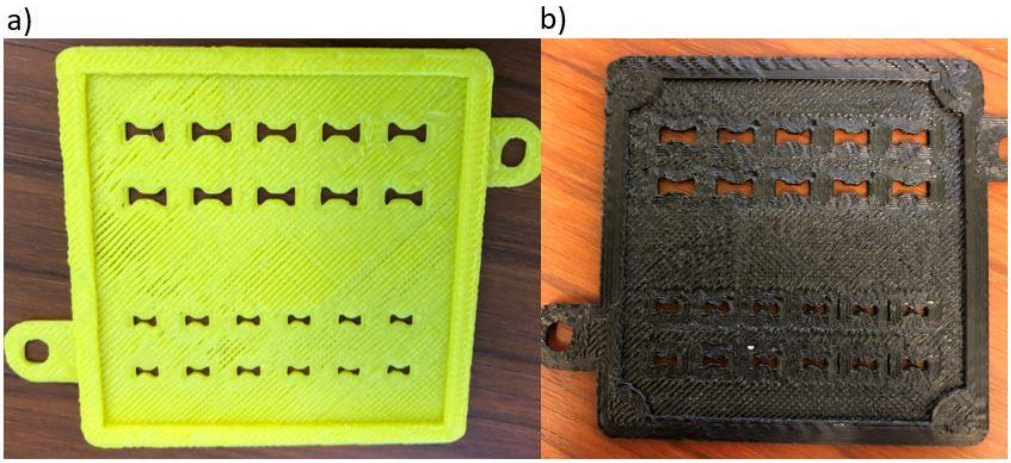

Figure 3.11 *3D Printed shadowmasks with Bow Tie filament design. Tabs on sides for mounting to Evaporator holder. PDMS well structures and NC would be set in indented portion.* ***a)*** *First iteration of Bow Tie design. No alignment used.* ***b)*** *Second iteration of Bow Tie design. Corners added to improve alignment.*

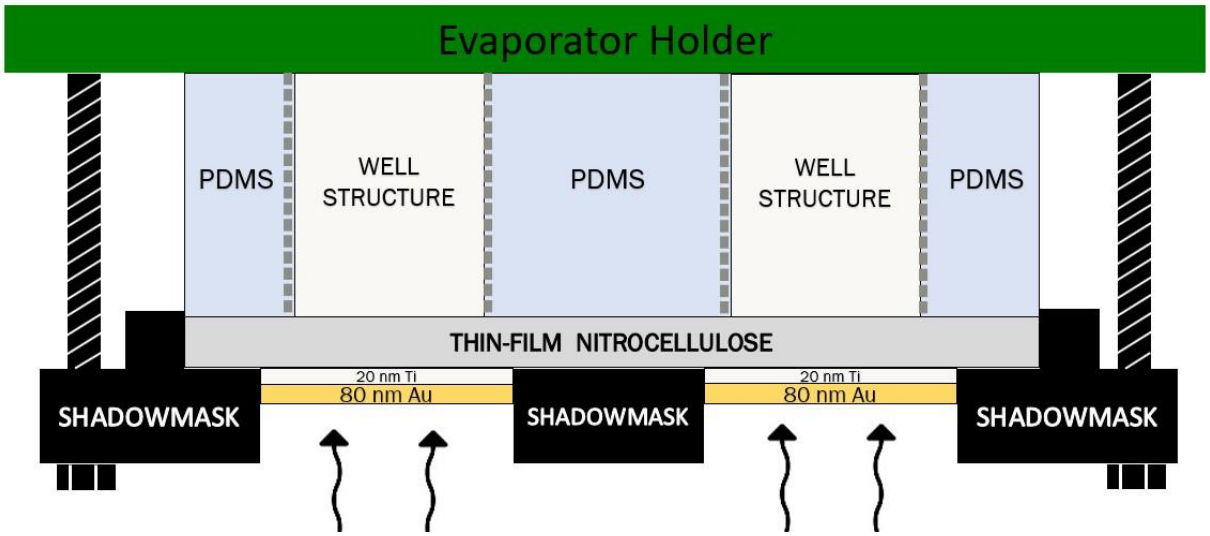

Figure 3.12 *Cross-sectional view of evaporator holder, NC/PDMS Well structures, and 3D printed shadowmask utilized to deposit Au/Ti on to NC.*

A Bow Tie design was chosen for two reasons. The first reason is to exploit the Au/Ti explosive decomposition seen in Section 4.2 with testing of NC directly on a substrate. To take advantage of

this decomposition, the thin part of the Bow Tie (middle) lies directly over the well structure. The size of the middle filament region was chosen to not fully cover the well structure. There is a need to determine if a chain reaction of thermal decomposition of NC occurs outside the Au/Ti filament region. If the well structure was fully covered, this analysis wouldn't be possible.

The second reason is to ensure good contact is made during testing. Outer, wider portions of the Bow Tie act as contact pads for probe application. The size of these contact pads was chosen based on test probes employed for this work.

As previously stated, three tests were performed with a Bow Tie design over well structures. Only 2 mm x 2 mm well structures were tested. Any 1 mm x 1 mm well structure was not a viable candidate for testing due to misalignment of Au/Ti filaments with well structures.

3.5 DESIGN CHALLENGES

Fabrication and manufacture of all constituent components do not use standard fabrication techniques. Each component required some form of alternative solution, fabrication tweak or outside the box type of thinking.

3.5.1 NON-STANDARD FABRICATION OF PDMS WELL STRUCTURES

The first challenge to be addressed was formation of PDMS well structures. Any PDMS fabrication method must be focused on making a master mold in which to pour PDMS. This master mold is used to form multiple iterations of structures. A couple of fabrication methods could be employed but one method ultimately was chosen for this work.

One of the methods used widely is utilized for microfluidic channels [36]. Using a photoresist such as SU-8 [37], standard photolithography could be used to create a master mold. For this work, rather than fabricate channels requiring only thin layers of SU-8, a very thick layer of SU-8 greater

than 1 mm would be needed to make through-hole or well structures. SU-8 2150 [38] is one of the thickest made and by looking at the datasheet, a single coat spun on a substrate at the lowest speed would yield just over 200 μm. To reach 1 mm, 5 coats of SU-8 would have to be processed by photolithography. This is simply not practical due to the fabrication times required. Therefore, an alternative method is required.

The second method to create a master mold for fabrication of PDMS well structures consists of milling a bulk piece of material to exact dimensions required. For this work, this is the method of choice. The limitation for this method is not an issue of how thick something could be made; rather how small the structures could be. The tooling size for a milling machine is not designed to work on a micron scale. Therefore, millimeter (mm) sized features were used for this work.

3.5.2 FABRICATION OF NITROCELLULOSE MEMBRANES

Uniform distribution of NC onto a substrate was obtained in a similar fashion to photoresists. It was done by spin-coating a colloidal mixture at a constant speed (RPM) on a commercial spin-coat machine. However, getting a mixture of sufficient viscosity was a challenge. Determination of this required multiple test runs to establish the right mixture. The results are shown and described in Section 5.1.

Another major challenge was transfer of NC from the spin-coated substrate to PDMS well structures. NC could not be easily removed from the substrate due to strong van der Waals forces. This led to use of electrochemically deposited Pt on the substrate before spin-coating of NC. Pt is a low adhesion metal which allows for relatively easy removal of NC from a substrate.

Now that NC could be removed, a glue was needed to bond the NC membrane to the PDMS well structures. However, not any glue will work. Any glue which is methacrylate-based will dissolve

NC. Therefore, the idea to use PDMS as the "glue" was tested and proven successful. PDMS bonds well to other PDMS and through trial and error, NC was able to be bonded to PDMS as well with sufficient quantities of PDMS "glue".

3.5.3 3D PRINTED SHADOWMASK FOR DEPOSITION OF FILAMENTS

A quick test determined that Ti as an adhesion layer (approximately 20 nm) and Au as the filament layer (approximately 80 nm) could be deposited directly on NC. However, normally for depositions, standard photolithography and masks would be used to outline an area for deposition. Then, after deposition, the photoresist would be removed via acetone. The challenge here is that NC dissolves in acetone. If the deposition was done, it would be wasted immediately after by photoresist removal. Therefore, an alternative method outside of standard photolithography needed to be established.

A shadowmask made by 3D printing would create the outline to control where the Au/Ti filament was deposited while also preventing damage to NC. Fabrication of a 3D printed shadowmask is described in Section 4.4 and two iterations of the shadowmasks are shown in Fig. 4.6.

This method proved to be successful because it produced testable structures and if a shadowmask required alteration, a quick rendering and printing could be performed. To change a shadowmask, about one hour was required to modify the design and 3D print a new shadowmask. For standard photolithography, the time for mask modification could be significantly longer depending on complexity of the structures.

4 TESTING OF NITROCELLULOSE AS A DECOMPOSITION MECHANISM AND PROTECTIVE MEMBRANE

Systematic testing of NC to understand the decomposition mechanism for our work will be discussed in this section. A previously mentioned, NC has a thermal decomposition temperature that can change depending on the nitrate content or the rate of change of local temperature applied. Additionally, the typical evaporation temperature of Au is known giving an understanding that as long as the local temperature of NC is significantly higher than the decomposition temperature, then the decomposition mechanism for this work will be successful.

Characterization of the energy applied to the Au/Ti filaments used to increase the local temperature is performed in this section but of great importance is the understanding that only a small percentage of opening is required for our decomposition mechanism to be effective. As long as the opening is larger than the molecular size of our target analyte, flow due to the pressure gradient will occur. For example, if our target analyte is glucose, then the opening must be larger than ~1 nm [56]. This is achievable with even a small opening. Albeit, flow will be minimal in this situation so a larger opening would be preferred. Once the opening begins, due to the pressure differential described later in Section 4.3, the NC will continue to open until pressure has been equalized. Therefore, it is known that a low energy will be needed to perform our end goal but a good characterization is still important.

4.1 TESTING SETUP

The overall goal of this work is to determine the response of NC when current is applied to filaments directly on top. Applying current to filaments in a controlled manner is difficult when the structure to be tested is flexible and compressible. The best method found in this work was to repurpose a probe station as a test bench.

Figure 4.1 shows probes applied to an Au/Ti filament ready for testing. Using specially made test probes made from small contact pads dipped in soft silver solder was essential to minimize any damage to NC and Au/Ti filaments while also allowing for ample contact area to apply current. The silver solder allowed for ample contact adhesion to the Au/Ti filament while also being soft enough to not damage the Au/Ti filament during testing.

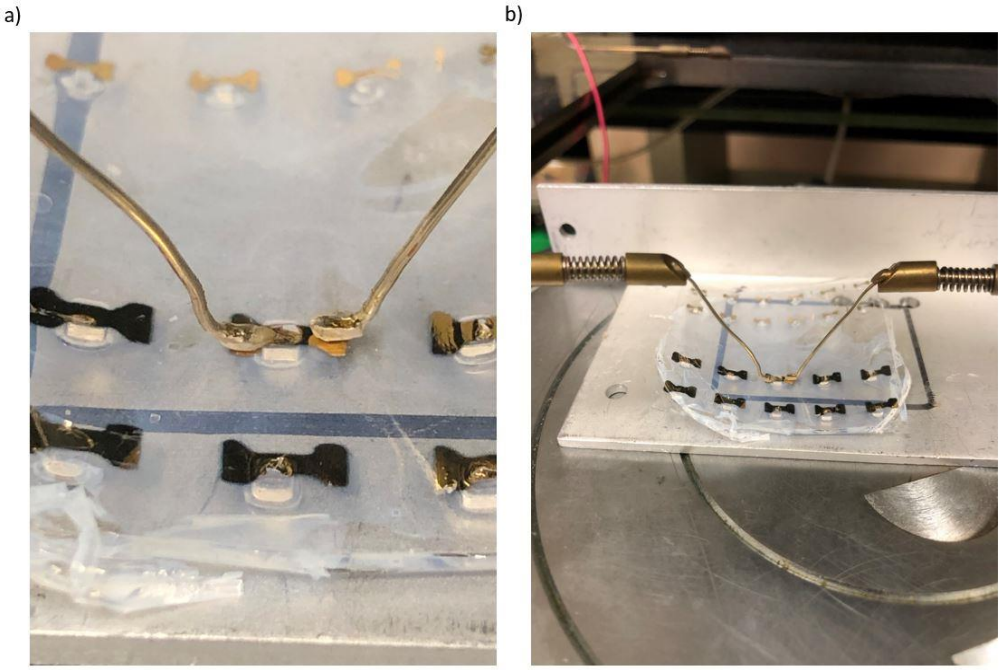

Figure 4.1 *Test Probes.* ***a)*** *Close-up view of Test Probes connected to Au/Ti filament.* ***b)*** *Expanded view showing all Bow Tie Au/Ti filaments deposited on NC.*

After determination of how to make reliable contact with Au/Ti filaments on NC, the next order of business was to create a controllable square wave pulse generator to apply current for a specific period of time. Several different designs were tested, including a capacitive pulse circuit, a stun gun circuit, and lastly a square wave pulse generator formed by Arduino Mega 2560 output and a power MOSFET. The last design proved to be the most controllable.

An Arduino Mega 2560 was programmed to send either an ON-state signal of 5V or OFF-state signal of 0V from an Arduino OUTPUT pin to the gate of an IRLZ24N Power N-MOSFET. This signal is only sent by an operator's push of a momentary pushbutton. If the ON-state signal is sent to the gate of the MOSFET, because voltage gate to source of 5V is higher than the threshold voltage, a channel is formed in the MOSFET between drain and source allowing current to potentially flow from drain to source. A separate power source is connected to one side of the Au/Ti filament. The other side of the Au/Ti filament is connected to a 0.1 Ω resistor used to perform a transient analysis of the Au/Ti filament. The 0.1 Ω resistor is then connected to the drain of the MOSFET. The source is connected to ground. The circuit for this can be seen in Fig. 4.2.

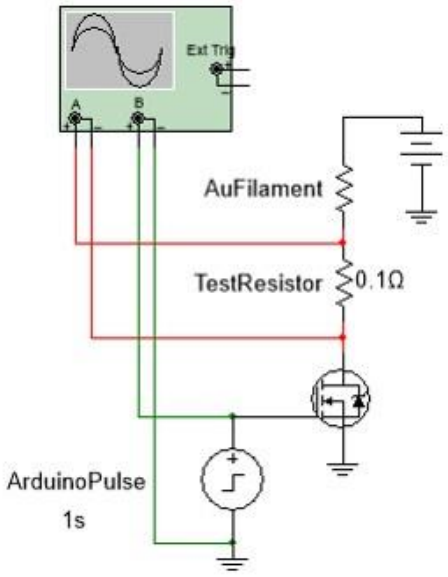

Figure 4.2 *Circuit for application of current to Bow Tie Au/Ti filaments.*

The Arduino output trigger produces a switching action that allows for controlled pulse generation. By programming the Arduino Mega 2560 to send a signal for a specified period of time, a square wave pulse generator is formed. The switch time of the Arduino Mega 2560 output, as seen in Fig. 4.3, takes 600 μs to switch from OFF to ON and also from ON to OFF. An illustration of all connections in the test bench is depicted in Fig. 4.4.

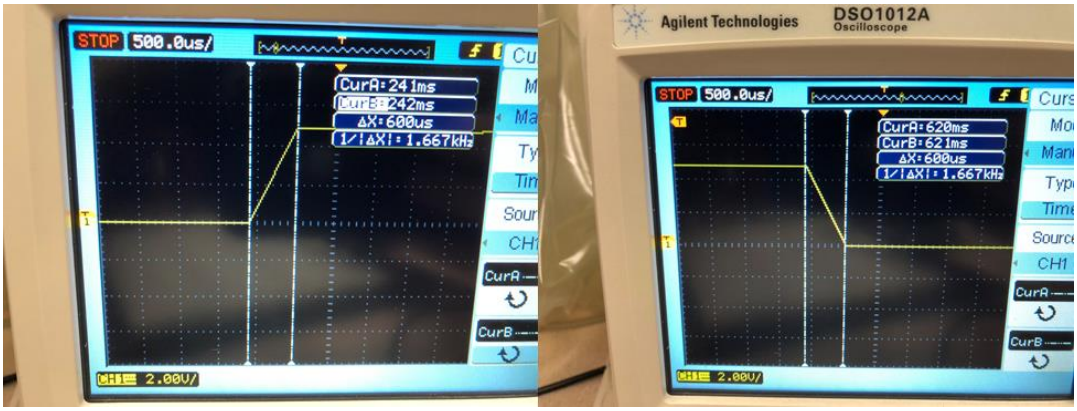

Figure 4.3 *Arduino Output pin response time of 600 µs OFF to ON and 600 µs ON to OFF.*

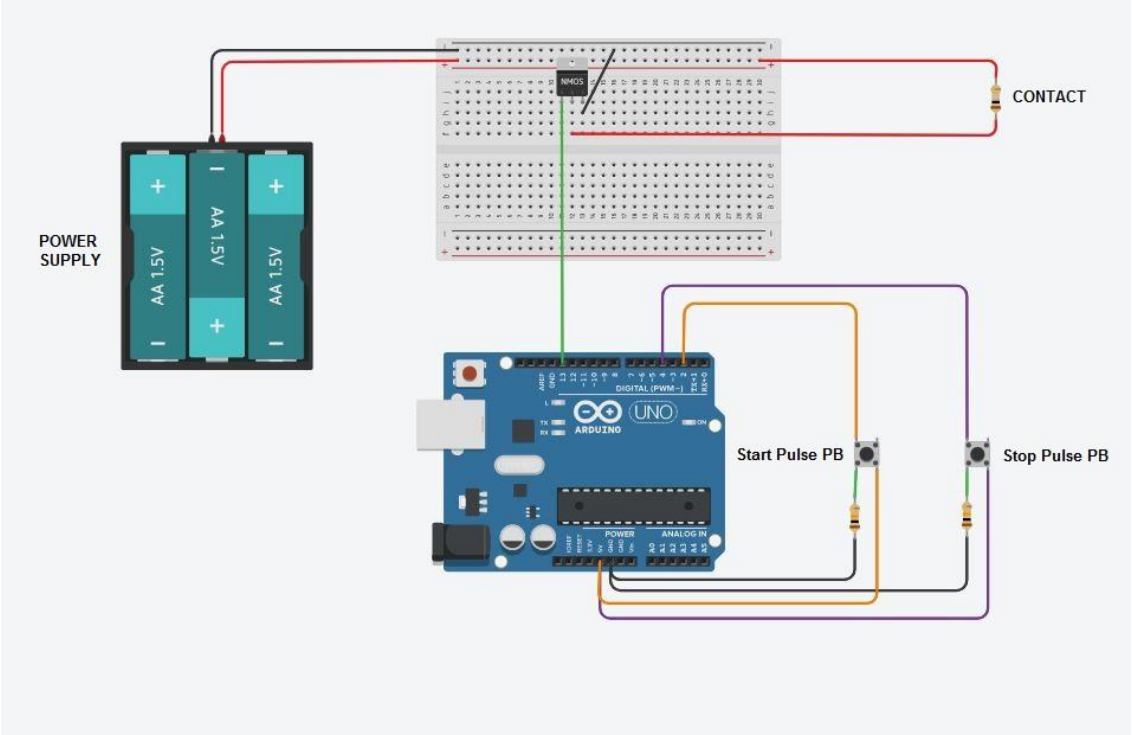

Figure 4.4 *Current test bench configuration.*

Programming of the Arduino Mega 2560 software [53], was achieved with the help of tutorials included in the Arduino software. Two of the tutorials (Blink and Button) were merged. Blink was designed to blink an LED using an output pin with a timer and delay and is used to turn the output pin ON and OFF for a specified period of time. The Button tutorial allows for a pushbutton to

trigger an output pin ON and OFF dependent on the position of the button. These formed the core of the program. In addition, a Graphical User Interface (GUI) shell was added to visually understand when the program was running and the actual amount of time it was running.

After the test bench was assembled, test parameters were required. To establish time required to decompose NC, the program was designed to start with a 1 s square wave pulse. The expectation is the Au/Ti explosive decomposing in less than 100 ms but sufficient time was given to ensure those results. If the Au/Ti filament explosively decomposes or NC decomposes, the test is terminated, because, most likely, the Au/Ti filament is registering as an open circuit and current would not flow. Therefore, there is no point in continued testing.

Monitoring of voltage output of the Arduino Mega 2560 and current flow through the Au/Ti filament are performed with an Agilent Technologies Oscilloscope. As previously mentioned, a 0.1 Ω resistor was placed in series with the Au/Ti filament, as shown in Fig. 4.2, with one channel of the oscilloscope measuring the voltage drop across that resistance as a function of time. By simply using Ohm's Law, the current response through the circuit can be ascertained.

4.2 TESTING DECOMPOSITION OF NITROCELLULOSE ON A SUBSTRATE WITH AU/TI FILAMENTS

Systematic testing of Au/Ti filaments on NC spin-coated onto a 2" Pt covered wafer was the first step. Three different thicknesses of NC were tested, 1.16, 1.89, and 2.52 μm for tests 1, 2, and 3, respectively. As mentioned previously, thickness variation is required to determine how NC thickness affects the activation energy required to thermally decompose NC.

The first step of this part of systematic testing is to spin-coat NC directly onto a 2" Pt covered Sapphire substrate (described in Section 3.2). For this test specifically, the NC was not transferred

to a PDMS well structure. Rather, Au/Ti filaments were deposited directly on the NC covered substrate.

The Au/Ti filaments were deposited atop NC in some arbitrary shape as performed per Section 3.4. 3D printed shadowmasks were developed in order to deposit specific shapes directly onto the NC. The reasoning for utilization of a 3D printed shadowmask is described in Section 4.5. A cross-sectional view of this experiment is shown in Fig. 4.5. The testing probes and experimental test bench are described in Section 4.1.

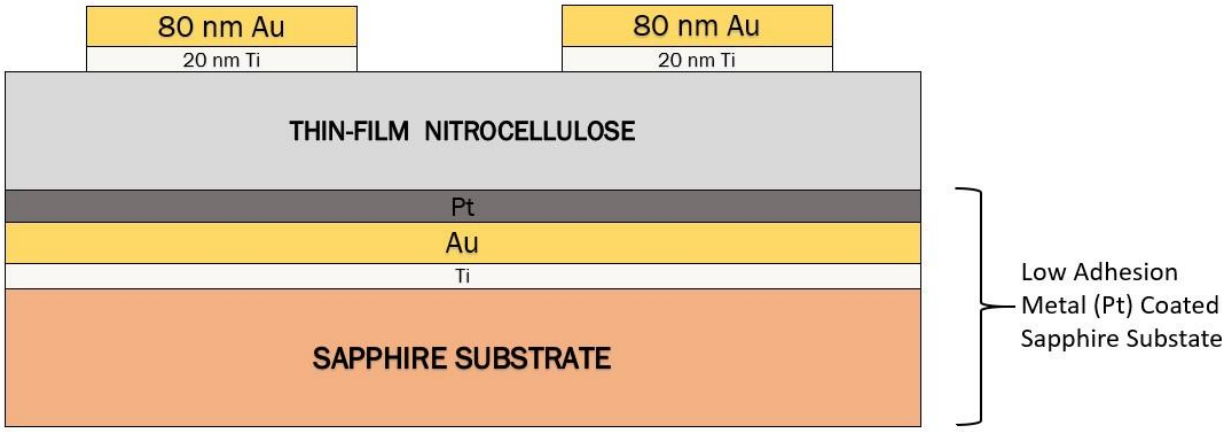

Figure 4.5 *Cross-sectional view of systematic testing of NC directly on wafer.*

For the shadowmask, a U-shaped 3D printed shadowmask was used and can be seen in Fig. 4.6. This shape was utilized in preliminary, less successful, iterations for decomposition of NC transferred to PDMS well structures. However, the shape required is arbitrary. The results expected from this testing would be similar even with the final design shown briefly in Section 3.4 and further described in Section 4.3.

The expectation of this part of testing is to act as a control for comparison with NC over PDMS well structures. It is not expected to decompose NC due to heat dissipation to the substrate. NC

requires a certain temperature to decompose and it is expected that a substrate would act as a heat sink.

Figure 4.6 *3D Printed shadowmask with U-Shaped filament pattern.*

Using the test bench described in Section 4.1, testing was performed of NC with Au/Ti filaments deposited. For testing of different thicknesses of NC, Fig. 4.5 visually represents the layered test setup shown in cross-sectional view shown above. The sole difference between each test is the thickness of NC which is difficult to discern the difference when only a micron of thickness separates each test. Therefore, only one systematic test picture is shown but this represents closely all three systematic tests. To measure NC thickness after spin-coat, refer to section 3.2 for the method.

For the Au/Ti filaments in this portion of systematic testing, resistance measurements ranged from 3.6 Ω to 9.4 Ω. Utilizing the test bench set-up prescribed in Section 4.1, systematic testing was performed. A visual representation of the results can be seen in Fig. 4.7, all of which were taken with an optical microscope of 5x, 10x, and 50x zooms from left to right, respectively.

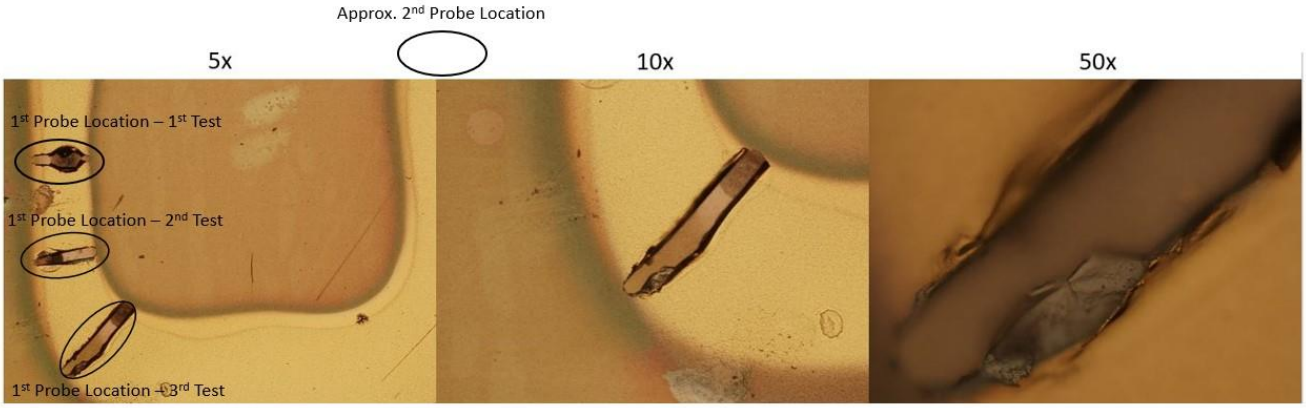

Figure 4.7 *Optical microscope pictures of exploded test points. From left, 5x zoom of filament over NC, middle of 10x zoom of filament over NC, and right 50x zoom of filament over NC. Left most picture shows three points of testing with identical results. Right most picture shows decomposed NC under Au/Ti filament.*

The most significant finding of this experiment is the location of the lines. Looking at the 5x optical microscope picture shown in Fig. 4.7, three burn lines can be seen. Each burn line was a location that the test probe was placed. The top most burn line was the first point of testing on this filament. The next test point was directly below and the last was the bottom burn line. Not shown in the 5x picture is the location of the second test probe which is out of the viewing field of the optical microscope. These burn lines all occurred when approximately 1 Amp of current was passed through the filament. Inspection of the 50x optical microscope image shows that the Au/Ti explosively decomposed and subsequently decomposed the NC directly underneath. When the Au/Ti explosively decomposed enough that the filament broke, decomposition of NC ceased. After the filament broke, no current was able to pass through the filament due to the open circuit created.

The results can be explained with two key points. The first is explained in Section 2.5. Thin-film and wire filaments explosively decompose when a significant enough amount of current is applied

to reach a large current density. As mentioned in the same section, the amount of current that is feasible before explosive decomposition of Au/Ti filaments is dependent on the cross-sectional area of the filament itself. The 3D printed shadowmask shown in Fig. 4.6 was designed to produce 1 mm wide filaments. Albeit, the precision of the shadowmask is low, we can still use this width to understand the results and proceed with further testing based on these results.

Given that a current density of $\approx 10^6$ A/cm^2 will result in explosive decomposition of Au and knowing the deposition thickness of Au is 80 nm, a maximum current before explosive decomposition can be calculated. The cross-sectional area is calculated by Eq. (4) and the current is calculated by Eq. (5).

$$Area = 1\,mm * 80\,nm = 8x10^{-7}\,cm^2 \tag{4}$$

$$I = J * A = 10^6 \frac{A}{cm^2} * 8x10^{-7}\,cm^2 = 0.8\,A \tag{5}$$

These calculations show that the approximate maximum potential that can be applied before explosive decomposition is 0.8 A. All testing of filaments with burn lines achieved a current density large enough to explosively decompose the Au/Ti filament. This leads to the second key point of why the Au/Ti filament explosively decomposed directly under the test probe and subsequently decomposing NC only in this location.

Localized application of the test probe allowed for the largest amount of joule heating to occur at this point. The wafer did act as a heat sink with exception of the localized area under the test probe. This heat formation allowed NC to reach temperatures high enough for decomposition. The explosive decomposition of Au/Ti must have triggered the NC decomposition until the point that enough Au explosively decomposed to achieve an open circuit.

Explosive decomposition of Au/Ti filaments is the method exploited for subsequent testing with NC over PDMS well structures. As proven by calculations, this allows for relatively low current and power to decompose NC while still having control. The next section will show testing of NC over PDMS well structures with a Bow Tie shape design to maximize decomposition of NC over each well structure.

4.3 TESTING DECOMPOSITION OF NITROCELLULOSE ATOP PDMS WELL STRUCTURES WITH AU/TI FILAMENTS

Systematic testing of Au/Ti filaments on NC transferred atop PDMS well structures was the next item to test. Three different thicknesses of NC were tested, 1.67, 2.42, and 2.98 μm for tests 1, 2, and 3, respectively. As mentioned previously, thickness variation is required to determine how NC thickness affects the activation energy required to thermally decompose NC.

We know that having even a small opening will be sufficient to allow biofluids to enter the well due to the pressure gradient between the well (~atmospheric pressure of 760 mmHg) and capillary hydrostatic pressure (~30 mmHg) [55]. Additional testing will be performed to determine the minimum required current to achieve sufficient introduction of biofluids.

The testing in this section is to prove that the amount of energy applied to the Au/Ti filaments directly correlates to the amount of thermal decomposition of the NC membranes. This will then correlate to a certain percentage of membrane opening. Additionally, thickness of the NC membrane changes the amount of energy required to thermally decompose the NC membrane.

In the previous section, it was determined that NC would undergo decomposition directly under the highest localized increase in temperature of the Au/Ti filament. Sufficient current was applied to each Au/Ti filament until current density was great enough for explosive decomposition the

filament. This leads to decomposition of NC locally which is the ideal response to be exploited for the second part of testing.

The first step for this part of systematic testing is to spin-coat NC directly onto a 2 in Pt covered Sapphire substrate. Next, NC was transferred to PDMS well structures. These steps are described in detail in Section 4.2.

The next step is deposition of Au/Ti filaments on NC as performed per Section 3.4. Two 3D printed shadowmasks as seen in Figure 3.10 were developed to deposit Bow Tie shapes directly onto NC over PDMS well structures. The first iteration was utilized for Bow Tie Tests 1 and 2. This yielded sufficient number of structures to be tested but alignment was an issue to be addressed. Therefore, the second iteration was made to address alignment concerns. This second iteration was utilized for Bow Tie Test 3 (discussed in Section 3.3).

A cross-sectional view or layer by layer depiction of PDMS well structures fabricated in section 3.1 all the way up to the Au/Ti filaments is shown in Fig. 4.8. The intermediary layer is NC with PDMS used as "glue" to transfer and hold NC to the PDMS well structures. Testing probes and an experimental test bench are described in Section 4.1.

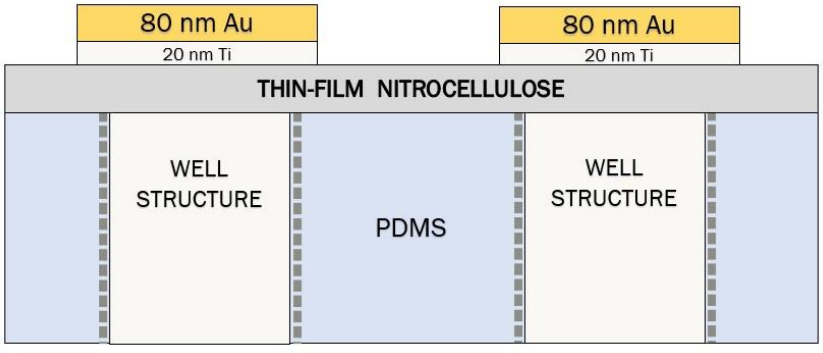

Figure 4.8 *Cross- sectional view of systematic testing of NC transferred to PDMS well structures. A* ***20 nm*** *of Ti acts as an adhesion layer between NC and an* ***80 nm*** *Au filament layer.*

The very first test is shown in Fig. 4.9 confirming the expected response. Comparison of two separate well structures is shown. Black squares illustrate locations of the well structure and indicate that the Au/Ti filaments are in fact covering a portion of the well structures. The conditions of the first test were straightforward. Resistance was measured to be 9.1 Ω for this filament. The current was chosen to be 0.5 A based on previous discussion about explosive decomposition of Au/Ti filaments. Using Ohm's Law, the voltage to apply to this filament would be 4.55 V. After setting the voltage on the test bench power supply to approximately 4.55 V, the Arduino push button was depressed. The first square pulse is 1 second long. This time was sufficient to explosively decompose the Au/Ti filament and subsequently decompose the NC beneath it. This can be seen in Fig. 4.9 with a comparison of an Au/Ti filament that is unopened and untested in Fig. 4.9a to the explosively decomposed filament and decomposed NC in Fig. 4.9b.

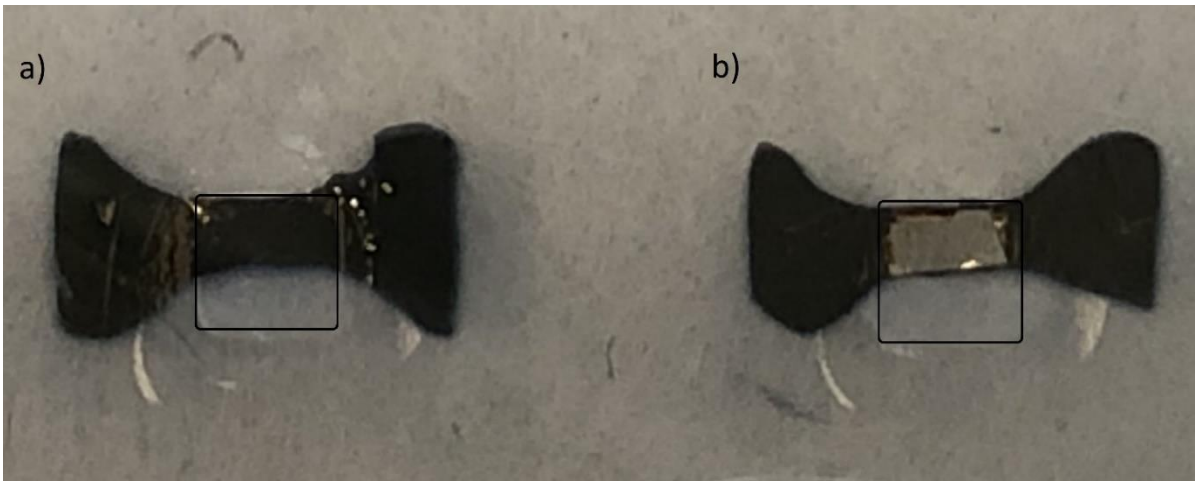

Figure 4.9 *Comparison of two filaments over PDMS well structures.* ***BLACK*** *squares show well area of PDMS structure.* ***a)*** *Unopened and untested filament over PDMS. Au/Ti filament and NC membrane still intact.* ***b)*** *Tested filament over PDMS. Au/Ti filament and NC membrane no longer intact resulting in an opening into the well structure.*

Continued testing was required after this success to determine a relationship between current applied to percentage opened of the NC over the well structure.

Using the same method of testing as the first test, first measure resistance, then choose current to apply, calculate voltage required using Ohm's Law, and then, lastly, apply current to filament. The number of tests for each set of PDMS well structures and NC membrane was based on number of viable Au/Ti filaments. As previously mentioned, only 2 mm x 2 mm well structures were utilized. For Bow Tie Test 1, five of the ten well structures provided viable filaments. For Bow Tie Test 2, four of the ten well structures were suitable for testing. For Bow Tie Test 3, seven of the ten well structures had viable filaments.

To find the percentage of NC opened, a unique method was applied. Making use of Web Plot Digitizer [54], normally utilized to reconstruct graphs or utilize data from those graphs, a certain feature of this was manipulated for measurement. This feature allows placement of data points to create a freeform polygon. After the polygon is connected, the software calculates area of the polygon. The output shows total perimeter in pixels (px) and area in px^2. After forming polygons for the NC opening and Au/Ti filament coverage, a ratio between the two could be made. As long as the picture is not modified, a correct ratio of areas can be established. Since this ratio is px^2/px^2, a method of quantifying percentage of opened NC to total Au/Ti filament coverage is harnessed. This method is illustrated in Fig. 4.10 and permits quantifiable results of current applied versus percentage opened of NC. This method does not produce very accurate measurements but does give an approximate percentage of opening for visual purposes. This is due to the inherent error in the program as well as the accuracy of the freeform polygon compared to the actual graph. Therefore, the accuracy could be ± 5% for each opening.

Once the method of quantifying the results has been established, further testing is performed. After the successful results shown earlier, a threshold current required to start opening NC must be determined. NC membrane thickness was measured to compare response between different thicknesses. All Bow Tie test results started with a pre-determined current. The first tests were at a current sufficiently low to not explosively decompose the Au/Ti filament and subsequently decompose the NC membrane. This is shown in graphs as 0% open.

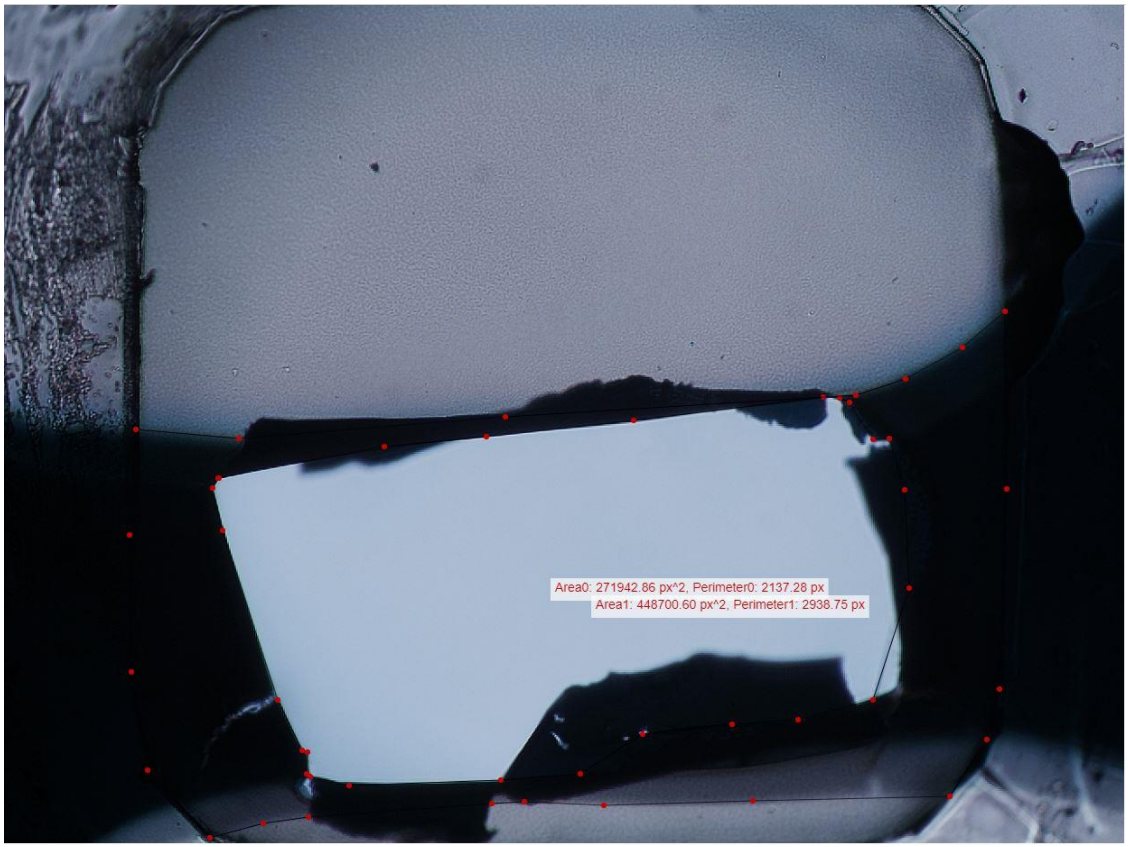

Figure 4.10 *Method to determine amount of PDMS well structure opened versus total filament coverage. Two freeform polygons made via Web Plot Digitizer [54]. Program calculates area in pixels^2. One polygon for area of opening and one for area of filament coverage.*

First, the Bow Tie test 1 (NC membrane thickness of 1.67 μm) results are shown in Fig. 4.11 for currents up to 0.5 A starting with the first result shown at current of 0.15 A. Each picture is analyzed as described above to determine the percentage of NC membrane opening versus the current applied.

Next, the Bow Tie test 2 (NC membrane thickness of 2.42 μm) results are shown in Fig. 4.12 for currents up to 0.3 A starting with the first result shown at current of 0.15 A.

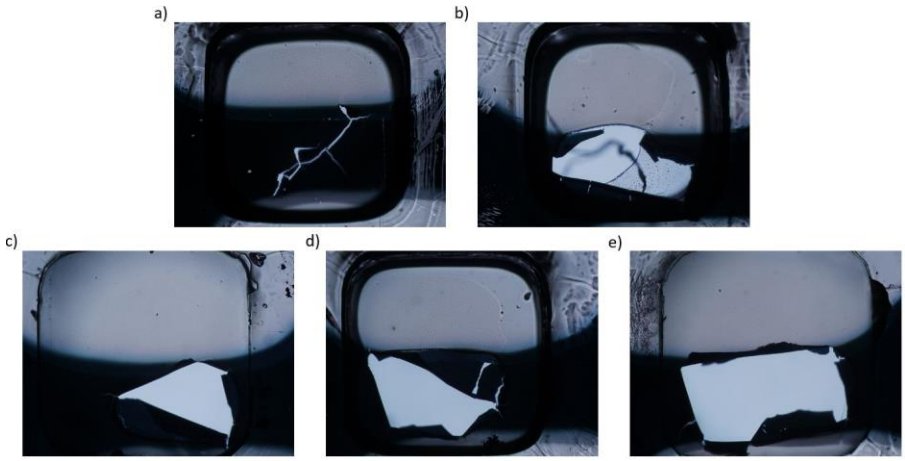

Figure 4.11 *Different percentages of NC membrane opening dependent on current applied. NC membrane thickness:* ***1.67 μm a)*** *Current applied to filament: 0.15 A. Deformation of NC but no opening.* ***b)*** *0.25 A* ***NOTE: first opening c)*** *0.30 A* ***d)*** *0.40 A* ***e)*** *0.50 A*

Lastly, the Bow Tie test 3 (NC membrane thickness of 2.98 μm) results are shown in Fig. 4.13 for currents up to 0.7 A starting with the first result shown at current of 0.2 A.

As seen from pictures shown in Figs. 4.11 – 4.13, a clear difference in opening size from one current to the next is evident. To quantify results, openings were measured as previously prescribed and plotted as a percentage of opening versus current and power in Figs. 4.14 and 4.15, respectively.

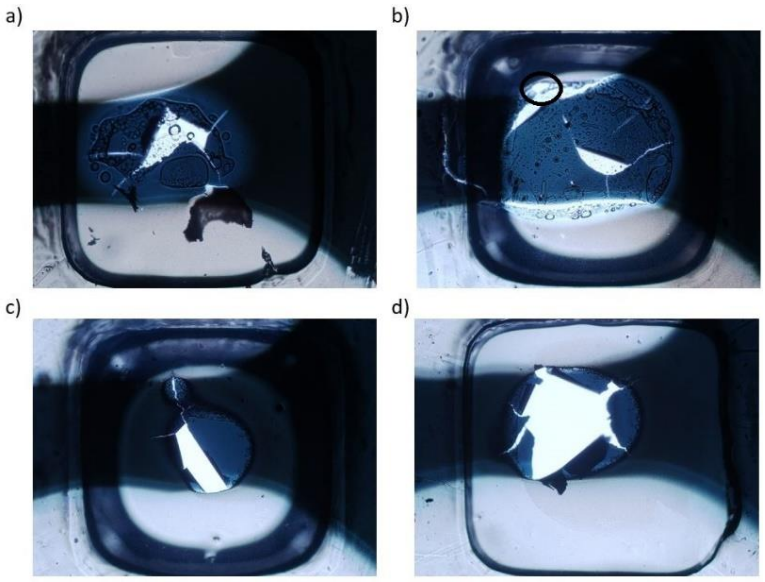

Figure 4.12 *Different percentages of NC membrane opening dependent on current applied. NC membrane thickness:* ***2.42 µm a)*** *Current applied to filament: 0.15 A. Deformation of NC but no opening.* ***b)*** *0.2 A.* ***NOTE: first opening*** *shown by small* ***BLACK*** *oval.* ***c)*** *0.25 A* ***d)*** *0.30 A*

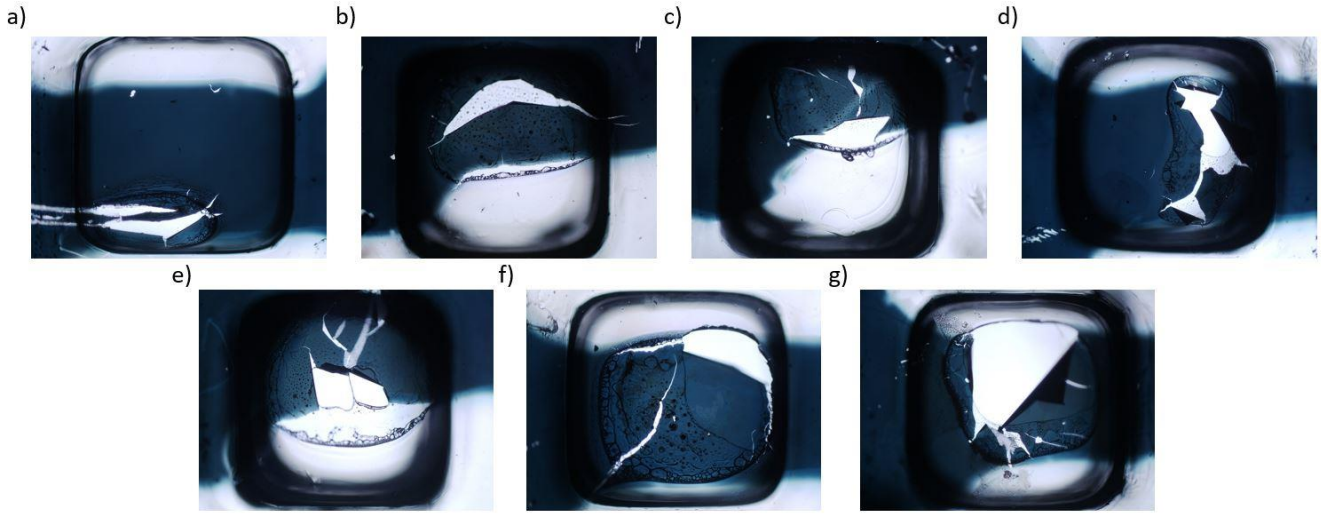

Figure 4.13 *Different percentages of NC membrane opening dependent on current applied. NC membrane thickness:* ***2.98 µm a)*** *Current applied to filament: 0.2 A. Deformation of NC and Au/Ti filament but no opening.* ***b)*** *0.25 A.* ***NOTE: first opening c)*** *0.35 A* ***d)*** *0.40 A* ***e)*** *0.50 A* ***f)*** *0.60 A* ***g)*** *0.70 A*

The blue dots on the first graph show Bow Tie test 1 results starting at 0.1 A. The trend shows that as current is increased, the percentage opened increases as well. A maximum achieved opening occurred at 0.5 A with a percentage opened slightly over 60%.

The red dots on the first graph show Bow Tie test 2 results starting at 0.15 A. The expected response for this test is that the thicker the NC membrane, the more energy required to cause decomposition of the NC membrane. We see that the threshold current for the point of NC membrane opening occurs with approximately 0.15 A applied versus the lower 0.1 A applied in Bow Tie test 1.

The green dots on the first graph show Bow Tie test 3 starting at 0.2 A. Similar to Bow Tie Test 2, the expectation is that the thicker the NC membrane, the more energy required to decompose. The threshold current for membrane opening is between 0.2 and 0.25 A. When approximately 0.2 A is applied to an Au/Ti filament, the Au/Ti filament explosively decomposes and deformation of the NC membrane is found, but no opening. However, at 0.25 A, the membrane is beginning to open.

The response related to energy versus thickness variation occurs as expected. Therefore, it is reasonable to assume that a thinner membrane would require less energy to cause decomposition.

The second graph for Bow Tie Tests 1, 2, and 3 shows calculated power for each current point shown in Fig. 4.15. Each individual filament resistance was used to calculate each power point. The trend of all tests show identical trends to that of the current vs percentage opened graph.

The last point to emphasize is the time required to explode or destroy the Au/Ti filament and subsequently cause decomposition of NC underneath. Figs. 4.16 shows a graph reconstructed from Agilent Technologies Oscilloscope waveforms during Bow Tie Test 3.

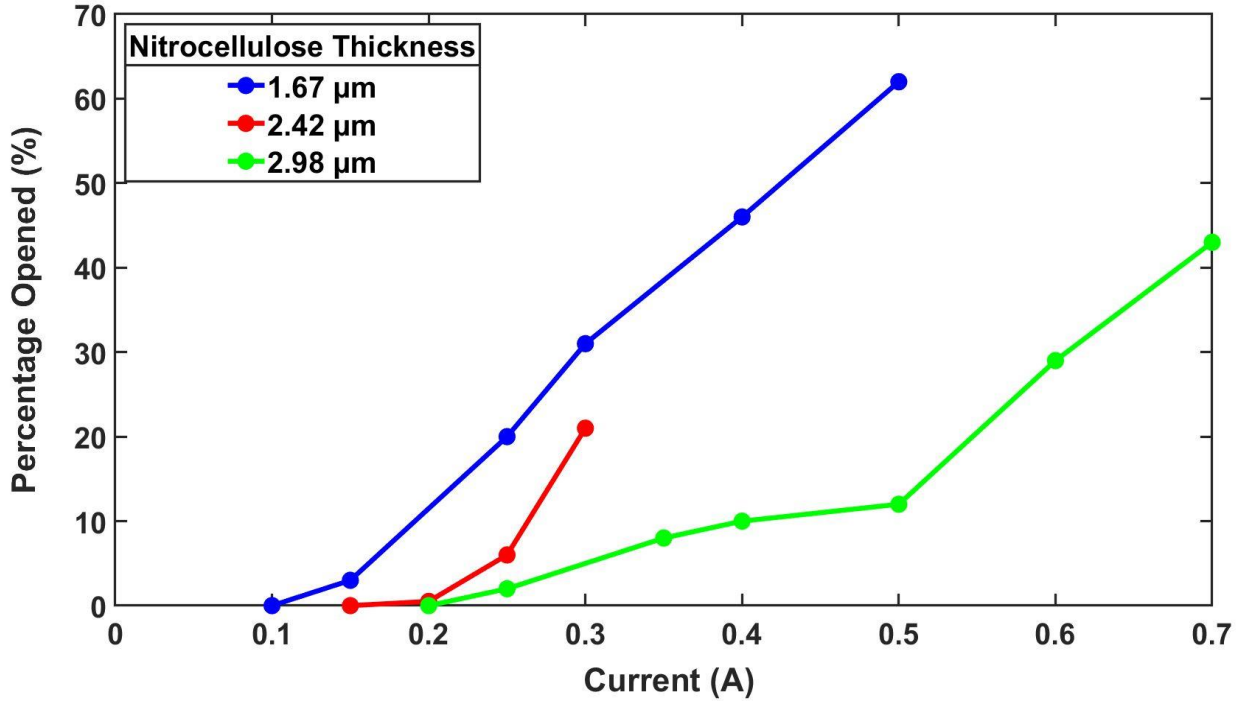

Figure 4.14 *Graph of percentage opened vs current (in A) applied.*

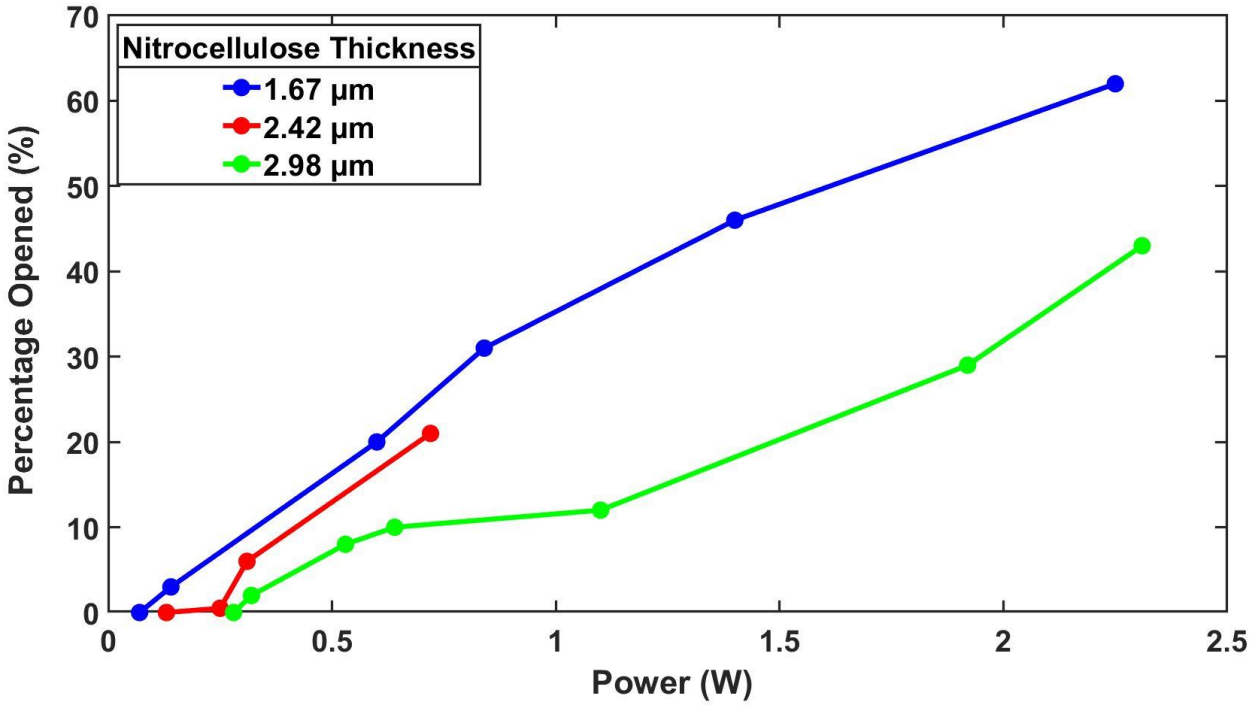

Figure 4.15 *Graph of percentage opened vs power (in W) applied.*

The blue line in the Fig. 4.16 graph shows when Gate voltage is applied to a Power MOSFET. The drain and source are connected to a power supply and the Au/Ti filament of concern. The voltage applied is arbitrary as long as the Gate voltage is greater than the Power MOSFET threshold voltage to turn it ON. Therefore, the blue line only represents when current is actually applied to the Au/Ti filament.

The red line in each graph shows the actual current response of the Au/Ti filament. The voltage drop across an inline 0.1 Ω resistor was used to quantify this current response. Direct measurement of the voltage drop across the Au/Ti filament would only show that the filament opens and then drops all voltage whereas the small resistor would drop very little when the Au/Ti filament opens. The reconstructed graph was converted to current for every point by using Ohm's Law.

The required amount of energy (in Joules) to destroy an Au/Ti filament and decompose NC can be extracted from these two graphs. To calculate the energy for the first graph, some information of the Au/Ti filament is required. This Au/Ti filament resistance was 4.4 Ω, voltage applied was 2.2 V and the current applied was approximately 0.5 A as evidenced by the first graph. To get energy, two things are required, Power and Time. The power can be calculated simply from current and voltage by:

$$P = I * V \tag{6}$$

and energy can be calculated from power (units of W or J/s) and time (in s). The calculation is as follows:

$$Energy = Power * Time \tag{7}$$

Given 0.5 A at 2.2 V, using Eq. 6, the power is 1.1 W. The time frame used is 50 ms shown by the first graph when current increases to when it stops. Therefore, from Eq. 7, the energy in Joules for this Au/Ti filament to be destroyed and NC to be decomposed is approximately 55 mJ of energy.

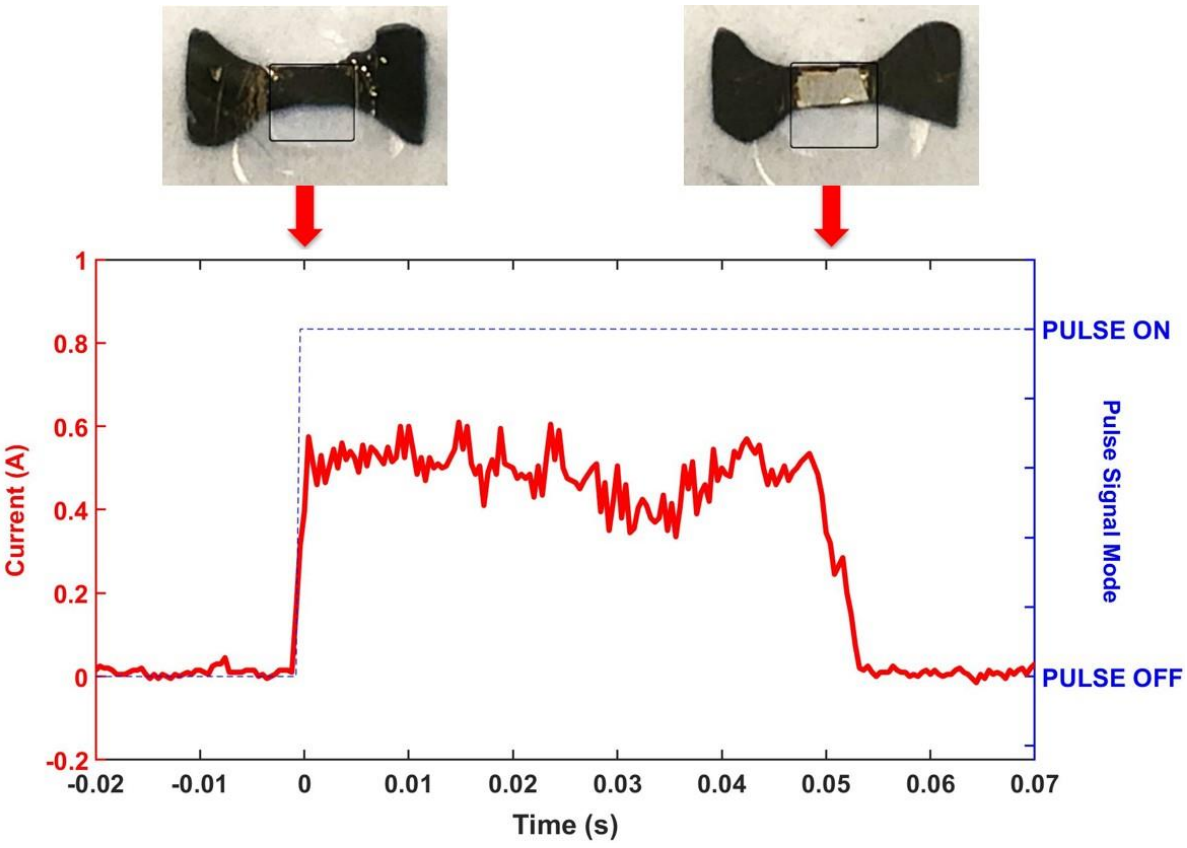

Figure 4.16 *Graph reconstructed from Oscilloscope measurement showing current transient analysis of an Au/Ti filament over a 2.98 µm thick NC membrane. Blue Line shows when an Arduino Output pulse signal is applied to the gate of a Power MOSFET allowing current to flow through the Au/Ti filament. Red Line shows the current transient analysis of the Au/Ti filament.* ***(0.5 A expected)****. Reduction in the current is observed at ≈ 50 ms indicating the onset of the filament decomposition. Arrows and visual representations of the Au/Ti response at t = 0s and t = ≈50 ms is shown above the transient analysis graph.*

Given the energy required to thermally decompose NC as described above and assuming that there will be some biofouling of the NC membrane, it can be expected that the actual energy required to open the well will be greater. With a fine layer of insulation applied to the filaments and NC membrane due to biofouling, the required activation energy to thermally decompose NC will be higher. Additionally, the longer the exposure to biofluids, the more biofouling that can be expected and therefore the more energy required. This could cause a potential issue with the lifetime of the batteries used in the circuit and could affect the overall functional lifetime of the biosensor array.

4.4 LEAK TESTING OF NITROCELLULOSE

Systematic testing of the porosity of NC was an important part of making this work useful in biomedical applications. Interaction of NC with Interstitial Fluid (ISF) or DI water must be confirmed. Initially, the NC sheets procured from ThermoFisher Scientific have a 0.2 μm pore size. The porosity after mixture with acetone and spin-coated is unknown. Therefore, a systematic test to check NC membranes and whether or not they leak is the topic of this section.

A cross-sectional schematic or layer by layer depiction of the experimental leak testing setup is shown in Fig. 4.17. Steps to fabricate 2 mm x 2 mm PDMS well structures and transfer spin-coated NC membranes is performed first, as described in Section 4.1. After the fabrication is complete, a methacrylate-based glue was to be utilized for gluing to a Si substrate. Glue was spread on the backside of the PDMS well structure with care taken not to interact with NC due to methacrylate having the same reaction with NC as acetone does with NC. After the appropriate amount of glue was distributed, either Toluidine Blue or Iodine Dye were placed inside the well structures. Finally, the Si substrate was connected to the PDMS well structures and allowed to dry for 1 hour. The glue was instant adhesive but extra time was given to ensure full drying before submersion of sample in DI water.

Fig. 4.18 shows the first initial test with the previously prescribed method of gluing. A randomly thick NC was utilized to determine the longevity of the glue used. This initial test was three hours in length and showed no degradation of either glue or NC.

Fig. 4.19 shows the first initial test with a PURPOSELY punctured NC membrane to visualize the flow of dye out of the well structure to the surrounding DI water. Wisps of dye can be seen coming from the 2 mm x 2 mm well structure.

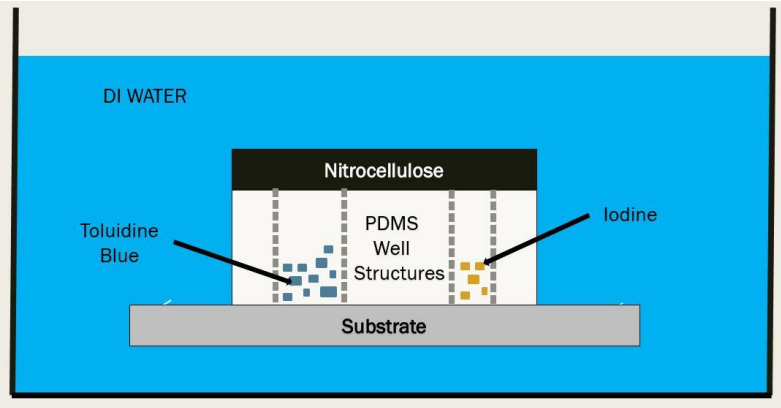

Figure 4.17 *Cross-sectional schematic of systematic leak testing of NC.*

Figure 4.18 *NC membrane over PDMS well structure with Blue Toluidine dye placed in well structure. Well structure, dye, and NC membrane glued to Si substrate. Submerged in DI water for 3 hours for initial testing.*

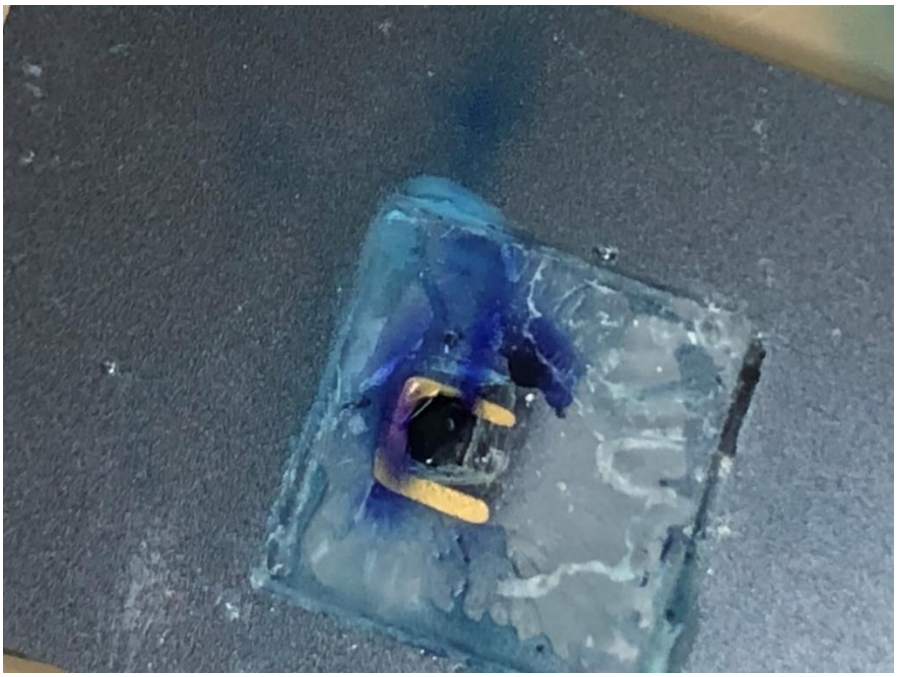

Figure 4.19 *Structure punctured to watch flow of dye through membrane into DI water.*

After the initial testing was shown to be successful, a longer test run was to be performed with varying thicknesses of NC applied to well structures. Fig. 4.20 shows three different samples with NC thicknesses of 2.68 μm, 2.82 μm, and 3.41 μm for Figs. 4.20a, 4.20b, and 4.20c, respectively.

The leak test with three different thicknesses of NC was performed for 1 week with Iodine dye and the results are promising. For each sample, the Iodine dye has leaked on the bottom side of the well structures between PDMS and substrate. The promising part is that NC has not punctured or leaked after 1 week. The glue on the bottom side does appear to be lifting off but with a better glue, a better seal can be made. However, it initially appears that NC will not leak. Further testing of samples long-term (> 3 month) must be performed to fully determine long-term porosity of NC membranes.

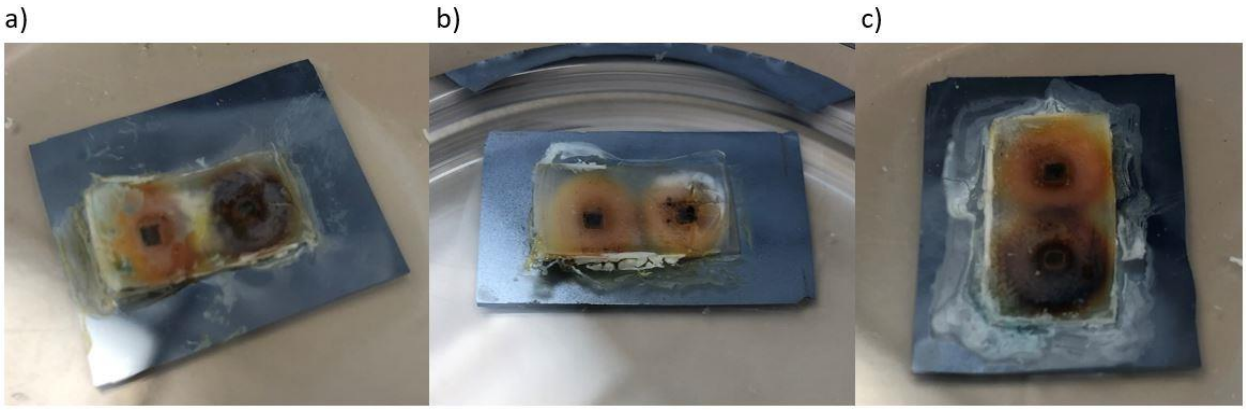

Figure 4.20 *NC membrane over PDMS well structure with Iodine dye placed in well structure. All samples submerged in DI water for 1 weeks for leak testing.* ***a)*** *NC thickness of 2.68 µm.* ***b)*** *NC thickness of 2.82 µm.* ***c)*** *NC thickness of 3.41 µm.*

A long-term modified leak test is currently underway as of March 16th, 2020. Fig. 4.21 shows the modified configuration. The main modification is the removal of a substrate to seal the opposite side of the PDMS well structure. As previously stated, one side is sealed and protected by a NC membrane and the other side is open to air. To seal the opposite side, the same mold utilized for initial PDMS well structure formation as described in Section 3.3 was employed. By using more PDMS material, the opposite side could be sealed. A visual representation of this can be seen in Fig. 4.22.

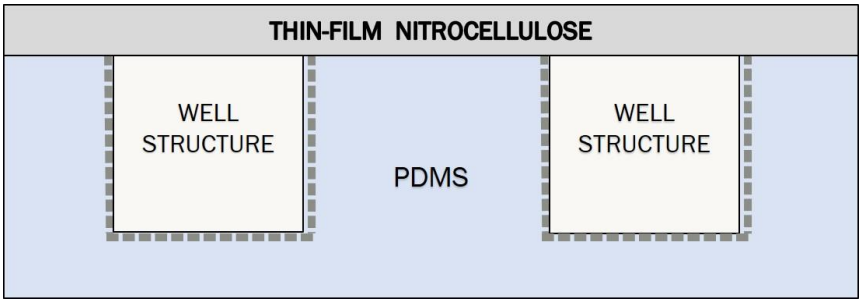

Figure 4.21 *Cross-sectional schematic of modified systematic leak testing of NC.*

Figure 4.22 *Realization of cross-sectional schematic as seen in Fig. 4.21 of modified PDMS well structures.*

After transfer of a NC membrane atop the open PDMS well structure, effectively sealing the well, it was then submerged in a DI water/Toluidine Blue fluid mixture as seen in Fig. 4.23.

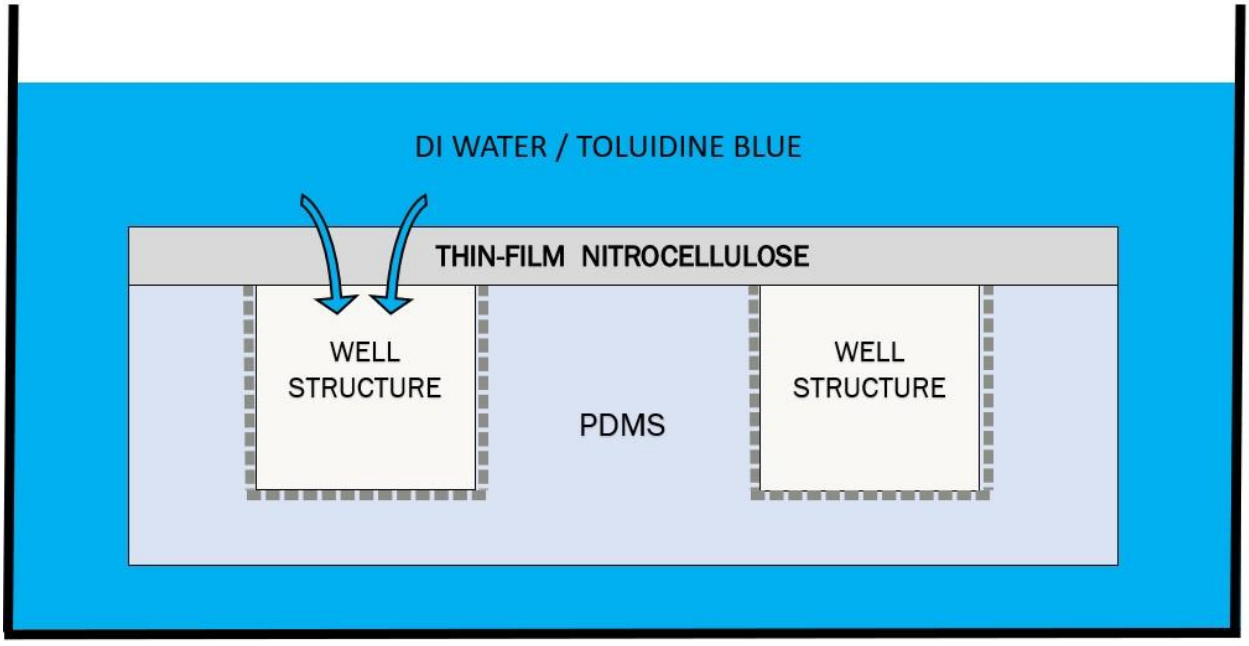

Figure 4.23 *Cross-sectional schematic of modified systematic leak testing of NC submerged in DI Water/Toluidine Blue fluid mixture.*

As of May 5, 2020, the NC membrane remains intact and no fluids have entered the PDMS well structure. Results of this can be seen in Fig. 4.24 and 4.25. No deformation or damage of the MC membrane has been evidenced. Continued monitoring will be done until mid-Summer 2020.

Figure 4.24 *NC membrane atop PDMS well structures. Samples submerged in DI Water/Toluidine Blue fluid mixture for 1.5 months for leak testing at time of publication.*

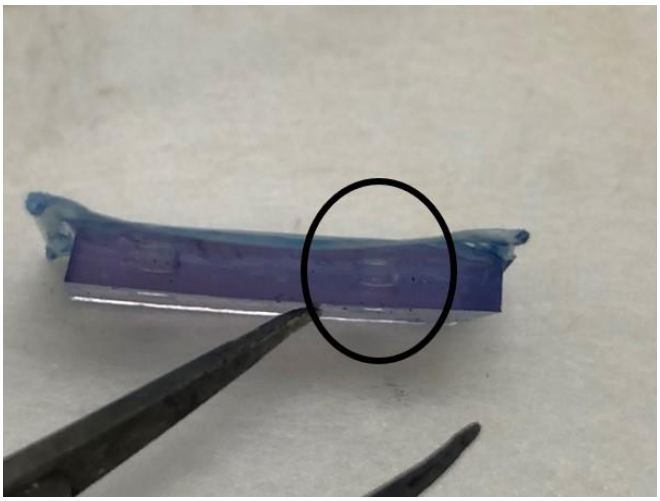

Figure 4.25 *Cross-sectional view of modified systematic leak testing of NC representing no introduction of fluid into the well structure.*

5 CONCLUSIONS

We have demonstrated the feasibility of electrically triggered decomposition of nitrocellulose membranes for on-demand activation of biosensors for long-term continuous health monitoring. An explosive decomposition of the Au/Ti filament caused by Joule heating results in the rupturing of the nitrocellulose membrane underneath the filament. This opening of the nitrocellulose membrane occurs within 50 ms allowing for exposure of a biosensor to biofluids. Additionally, 50 ms is sufficiently short to prevent local heating of surrounding tissues and therefore is not a danger to a potential patient.

A moderate current around 0.5 A with calculated energy of 55 mJ was shown to give a 13% opening of the relatively thicker, 2.98 μm thick nitrocellulose membrane compared to the original Au filament coverage. The experiments performed in air show that the application of electrical energy as low as 7 mJ to the filament placed on the top of 1.67 μm membrane is sufficient to initiate its opening. It is expected that even smaller amount of energy would be required for rupturing thinner membranes.

Our end goal of fabricating an array of biosensors to increase the overall functional lifetime for reduction of out-of-pocket patient costs and reduction of overall patient discomfort is one step closer. Given a moderate current of 0.5 A and assuming a 50 ms opening time, only 6.9 μAh will be required to open each well. Given a small watch battery has a rating from 100 – 200 mAh, an array of 10 biosensors with 14-day functional lifetime per biosensor would certainly be reasonable.

6 FUTURE WORK

Future work will include multiple different inclusions to the current work. Firstly, further testing with Au/Ti filaments and test structures submerged in fluid is needed to verify amount of energy required to cause nitrocellulose membrane decomposition. Next, we know that NC is biocompatible due to its nature of use in western blot testing but biocompatibility of NC long-term with in vivo implantation must still be performed. Also, long-term leak testing needs to be performed to determine if any flow of biofluid through the thin film of nitrocellulose into the well structure occurs. Along with the long-term leak testing, the pore size of NC pre-mixture and post-mixture can be compared by using a high-resolution SEM. This will help determine the potential of NC as a protective membrane. Lastly, thinner NC membranes must be produced to further minimize energy required to open each well.

REFERENCES

[1] A. St John and C.P. Price, “Existing and Emerging Technologies for Point-of-Care Testing”, *Clin Biochem Rev.*, vol. 35, pp.155–167, 2014.

[2] “Diabetes”, *World Health Organization,* [Online]. Available: https://www.who.int/news-room/fact-sheets/detail/diabetes, 2018.

[3] International Diabetes Federation. *IDF Diabetes Atlas, 8th edn.* Brussels, Belgium: International Diabetes Federation, 2017.

[4] L.C. Clark and C. Lyons Jr., “Electrode systems for continuous monitoring in cardiovascular surgery,” *Ann. N. Y. Acad. Sci.*, vol. 102, pp. 29–45, 1962.

[5] E. Yoo and S. Lee, “Glucose biosensors: An overview of Use in Clinical Practice,” *Sensors*, vol. 10, no. 5, pp. 4558–4576, 2010.

[6] Freestylelibre.us., *Freestyle Libre 14-Day System | Glucose Sensor & Reader | Freestylelibre.us*. [online] Available at: https://www.freestylelibre.us/system-overview/freestyle-14-day.html, 2020.

[7] L. Burton., “Diabetes patients hit by glucose monitor shortage.” *BBC News*, [online] Available at: https://www.bbc.com/news/business-51262846, 2020.

[8] Eversensediabetes.com, *Eversense Continuous Glucose Monitoring | Long-Term Continuous Glucose Monitor*, [Online]. Available at: https://www.eversensediabetes.com, 2020.

[9] J. Santini, M. Cima and R. Langer, "A controlled-release microchip", *Nature*, vol. 397, no. 6717, pp. 335-338, 1999.

[10] J. Credou, R. Faddoul, and T. Berthelot, Photo-assisted inkjet printing of antibodies onto cellulose for the eco2-friendly preparation of immunoassay membranes. *RSC Advances*, vol. 5, no.38, pp.29786–29798, 2015.

[11] A. Li, Y. Wang, L. Deng, X. Zhao, Q. Yan, Y. Cai, J. Lin, Y. Bai, S. Liu, and Y. Zhang, "Use of nitrocellulose membranes as a scaffold in cell culture", *Cytotechnology*, vol. 65, no.1, pp.71–81, 2012.

[12] J.M Maloney, S.A. Uhland, B.F. Polito, N.F. Sheppard Jr., C.M. Pelta, and J.T. Santini Jr., "Electrothermally activated microchips for implantable drug delivery and biosensing," *J Control Release*, vol. 109, pp. 244–255, 2005.

[13] N. Bhalla, P. Jolly, N. Formisano, and P. Estrela, "Introduction to biosensors," *Essays in Biochemistry*, vol. 60, no. 1, pp. 1–8, 2016.

[14] S. Rubenwolf, S. Kerzenmacher, R. Zengerle, and F. von Stetten, "Strategies to extend the lifetime of bioelectrochemical enzyme electrodes for biosensing and biofuel cell applications", *Applied Microbiology and Biotechnology*, vol. 89, no. 5, pp.1315–1322, 2010.

[15] C. Karunakaran, K. Bhargava, and R. Benjamin, *Biosensors and Bioelectronics*. 1st ed. Waltham, MA: Elsevier, pp. 2–16, 2015.

[16] C. Karunakaran, K. Bhargava, and R. Benjamin, *Biosensors and Bioelectronics*. 1st ed. Waltham, MA: Elsevier, pp. 135–144, 2015.

[17] L. Fang, B. Liang, G. Yang, Y. Hu, Q. Zhu, and X. Ye, "Study of glucose biosensor lifetime improvement in 37°C serum based on PANI enzyme immobilization and PLGA biodegradable membrane" *Biosensors and Bioelectronics*, vol. 56, pp. 91–96, 2014.

[18] L. Low, S. Seetharaman, K. He, and M. Madou, "Microactuators toward microvalves for responsive controlled drug delivery", *Sensors and Actuators B*, vol. 67, no. 1, pp. 149–160, 2000.

[19] E.F. Panarin, K.K. Kalninsh, and D, Pestov, "Complexation of hydrogen peroxide with polyvinylpyrrolidone: Ab initio calculations", *European Polymer J.* vol. 37, no. 375, 2001.

[20] R. Hurk, and S. Evoy, “A Review of Membrane-Based Biosensors for Pathogen Detection”, *Sensors*, vol. 15, no. 6, pp.14045–14078, 2015.

[21] M.A. Fernandez de la Ossa, M. Torre, C. García-Ruiz, “Nitrocellulose in propellants: Characteristics and thermal properties”. *Advances in Materials Science Research*, Nova Science Publishers: Hauppauge, NY, USA, 2012, vol. 7, pp. 201–220. ISBN 978-1-61209-821-0.

[22] A. Yetisen, M. Akram, C. Lowe, “Paper-based microfluidic point-of-care diagnostic devices”, *Lab on a Chip*, vol. 13, no. 12, p.2210, 2013.

[23] C. Saunders and L. Taylor, "A review of the synthesis, chemistry and analysis of nitrocellulose", *Journal of Energetic Materials*, vol. 8, no. 3, pp. 149-203, 1990.

[24] "Gunpowder | Facts, History, & Definition", *Encyclopedia Britannica*, [Online]. Available: https://www.britannica.com/technology/gunpowder, 1998.

[25] "Nitrocellulose | chemical compound", *Encyclopedia Britannica*, [Online]. Available: https://www.britannica.com/science/nitrocellulose, 1998.

[26] C. Fordyce, "Improved Safety Motion Picture Film Support", *Journal of the Society of Motion Picture Engineers*, vol. 51, no. 4, pp. 331-350, 1948.

[27] "Applications and Characterization of Nitrocellulose", *AZoM.com*, [Online]. Available: https://www.azom.com/article.aspx?ArticleID=2785, 2005.

[28] "Western blot | Learn Science at Scitable", *Nature.com*, [Online]. Available: https://www.nature.com/scitable/definition/western-blot-288/, 2014.

[29] "Nitrocellulose Membrane, 0.2 µm, 7.9 cm x 10.5 cm", [Online]. Available: https://www.thermofisher.com/order/catalog/product/88013#/88013, 2019.

[30] V. Nadkarni and S. Samant, "Spin coating technique for the preparation of thin nitrocellulose films for solid state nuclear track detection", *Radiation Measurements*, vol. 27, no. 3, pp. 505-510, 1997.

[31] "Cellulose Derivatives", *Polymerdatabase.com*, [Online]. Available: https://polymerdatabase.com/polymer%20classes/Cellulose%20type.html, 2015.

[32] M. Shelton, "Cellulose Esters, Inorganic Esters", *Kirk-Othmer Encyclopedia of Chemical Technology*, 2003.

[33] T. Urbanski, "Chemistry and Technology of Explosives", *Science*, Pergamon Press, New York, NY, vol. 2, pp. 321, 1964.

[34] Ibid, p. 327.

[35] G. Wilson and F. Miles, "The Solvation of Nitrocellulose in Acetone-Water Mixtures", *Philosophical Transactions of the Royal Society A: Mathematical, Physical and Engineering Sciences*, vol. 233, no. 721-730, pp. 247-277, 1934.

[36] Q. Luo, T. Ren, H. Shen, J. Zhang and D. Liang, "The Thermal Properties of Nitrocellulose: From Thermal Decomposition to Thermal Explosion", *Combustion Science and Technology*, vol. 190, no. 4, pp. 579-590, 2017.

[37] W. Groenewoud, "DIFFERENTIAL SCANNING CALORIMETRY", *Characterization of Polymers by Thermal Analysis*, pp. 10-60, 2001.

[38] C. Jose Chirayil, J. Abraham, R. Kumar Mishra, S. George and S. Thomas, "Instrumental Techniques for the Characterization of Nanoparticles", *Thermal and Rheological Measurement Techniques for Nanomaterials Characterization*, pp. 1-36, 2017.

[39] W. Groenewoud, "THERMOGRAVIMETRY", *Characterization of Polymers by Thermal Analysis*, pp. 61-76, 2001.

[40] S. Pourmortazavi, S. Hosseini, M. Rahimi-Nasrabadi, S. Hajimirsadeghi and H. Momenian, "Effect of nitrate content on thermal decomposition of nitrocellulose", *Journal of Hazardous Materials*, vol. 162, no. 2-3, pp. 1141-1144, 2009.

[41] Lesker.com, *Gold (Au) Pellets Evaporation Materials*., [Online]. Available at: https://www.lesker.com/newweb/deposition_materials/depositionmaterials_evaporationmaterials_1.cfm?pgid=au1, 2020.

[42] T. Tucker, "Behavior of Exploding Gold Wires", *Journal of Applied Physics*, vol. 32, no. 10, pp. 1894-1900, 1961.

[43] I. Karimkhodzhaev and M. Martynyuk, "Oscillographic study of electrical explosion in copper and gold", *Journal of Applied Mechanics and Technical Physics*, vol. 15, no. 3, pp. 330-333, 1975.

[44] M. Aguilar, A. Oliva and P. Quintana, "The effect of electrical current (DC) on gold thin films", *Surface Science*, vol. 409, no. 3, pp. 501-511, 1998.

[45] M.K Marakhtanov and A.M Marakhtanov, "Electrical explosion of cold thin metal films", *Thin Solid Films*, Vol. 359, No. 2, pp. 127-135, 2000.

[46] Y. Li et al., "In vivo release from a drug delivery MEMS device", *Journal of Controlled Release*, vol. 100, no. 2, pp. 211-219, 2004.

[47] K. Kim, K. Kim, and S. Jang, "Bridge Burst Characteristics of Aluminum and Copper Thin-Film Bridges in Electrical Initiation Devices", *Korean Journal of Metals and Materials*, vol. 56, no. 3, 2018.

[48] Y. Xia and G. Whitesides, "Soft Lithography", *Angewandte Chemie International Edition*, vol. 37, no. 5, pp. 550-575, 1998.

[49] "SYLGARD™ 184 Silicone Elastomer", *Dow.com*, [Online]. Available: https://www.dow.com/content/dam/dcc/documents/en-us/productdatasheet/11/11-31/11-3184-sylgard-184-elastomer.pdf?iframe=true, 2019.

[50] "DuPont and Haas, Shipley SPR™3000 photoresist | Kayaku", *Kayaku Advanced Materials, Inc.*, [Online]. Available: https://kayakuam.com/products/megaposit-spr3000-series-photoresists/, 2019.

[51] "SU-8 2000 - i-Line resists for fabricating micro/nano structures", *Kayaku Advanced Materials, Inc.*, [Online]. Available: https://kayakuam.com/products/su-8-2000/, 2019.

[52] *Microchemicals.com*, [Online]. Available: https://www.microchemicals.com/micro/tds_az_p4000_series.pdf, 2019.

[53] "Arduino – Built in Examples", *Arduino.cc*, [Online]. Available: https://www.arduino.cc/en/Tutorial/BuiltInExamples, 2019.

[54] "Web Plot Digitizer", [Online]. Available: https://automeris.io/WebPlotDigitizer/, 2019.

[55] A. Darwish, F. Lui, Physiology, Colloid Osmotic Pressure, Treasure Island (FL): StatPearls Publishing, 2020.

[56] Bionumbers.hms.harvard.edu, *Size of Glucose Ring Molecule - Generic - BNID 110368*, [Online]. Available at: https://bionumbers.hms.harvard.edu/bionumber.aspx?&id=110368, 2020.

APPENDIX A

1. Apply the following steps to produce NC membranes on a low adhesion metal (Pt) coated 2” silicon or sapphire substrate:
    a. Weigh pre-cut NC sheet to determine appropriate W/V ratio for required thickness needed.
        i. For example, if ≈ 2μm thickness is required, continue following the procedure. Otherwise adjust acetone volume and spin speeds as described in Section 5.1.
    b. Using a full pre-cut NC sheet, fold and place into small beaker (≈40 mL).
    c. Fill small beaker with acetone to 10 mL line.
    d. Using stirring rod or pipette tube, mix solution of acetone and NC sheet for 3 minutes. Mixture should have no fragments floating and should be clear. If no fragments, skip to part g.
    e. If fragments remain, mix for 1 additional minute. Repeat as necessary until all fragments dissolved.
    f. Place and center 2” Pt covered substrate on spin coater and turn vacuum ON.
    g. Using pipette, put approximately 4 mL of mix onto Pt covered substrate ensuring entire substrate is covered.
    h. Wait 1 minute.
    i. Spin coat mix at 1000 RPM for 15 seconds with an acceleration of 500 RPM/sec.

j. Air dry for 5 minutes.

k. Check thickness with profilometer.

APPENDIX B

1. Utilizing previous spin-coated NC membranes, apply the following steps to transfer NC membranes to PDMS well structures:

    a. Perform procedure in [40] with 0.5 grams Base to 0.05 grams curing agent and mix to create “glue” to make solid contact between PDMS well structures and NC membranes.

    b. Carefully spread “glue” from step 1a on PDMS well structures. **Ensure PDMS does not enter well structures**.

    c. Carefully apply PDMS well structures to spin-coated NC membrane.

    d. Place heavy object on PDMS well structures to evenly distribute to NC membrane.

    e. Allow 48 hours to dry if ambient temperature drying is required. Drying can be sped up by placing on hot plate at 50°C for 24 hours.

    f. Peel NC and PDMS well structures from Pt covered substrate. This should come off easily. Cut using razor blade as necessary.